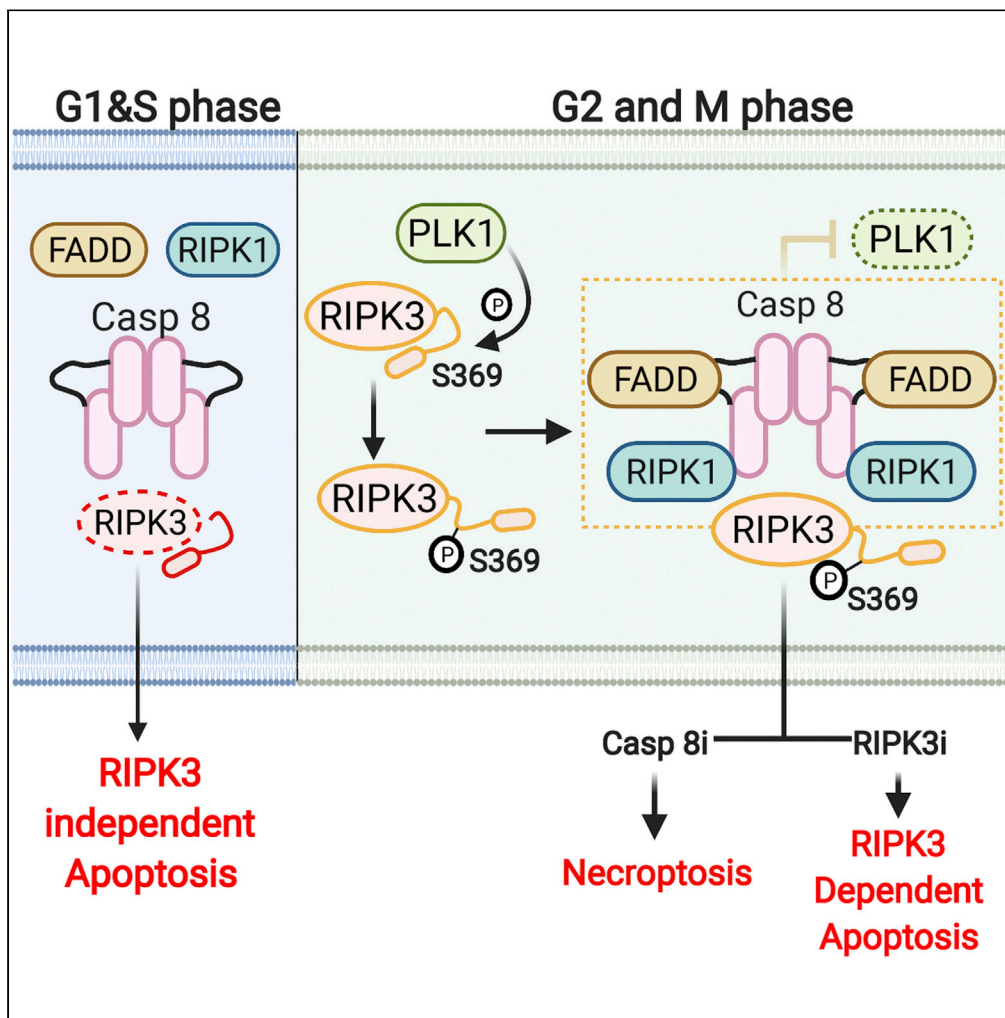


Article

PLK1-mediated S369 phosphorylation of RIPK3 during G2 and M phases enables its ripoptosome incorporation and activity



Kartik Gupta, Bo Liu

liub@surgery.wisc.edu

Highlights

Inhibiting RIPK3, a necroptotic kinase, triggers apoptosis via the ripoptosome

Ripoptosome normally cleaves RIPK3 and is assembled in mitosis

pS369 in G2/M phases prevents RIPK3 proteolysis via ripoptosome

Phosphorylation of S369 by PLK1 enables cell death plasticity in G2/M phases

Gupta & Liu, iScience 24, 102320  
April 23, 2021 © 2021 The Author(s).  
<https://doi.org/10.1016/j.isci.2021.102320>



## Article

## PLK1-mediated S369 phosphorylation of RIPK3 during G2 and M phases enables its ripoptosome incorporation and activity

Kartik Gupta<sup>1</sup> and Bo Liu<sup>1,2,3,\*</sup>

## SUMMARY

Receptor-interacting protein kinase 3 executes a form of regulated necrosis called necroptosis. Upon induction of an altered conformation by chemical inhibitors or via mutations in its kinase site, RIPK3 associates with a multiprotein complex called the ripoptosome—a signaling platform containing FADD, RIPK1, caspase 8, and cFLIP—and becomes decisive in the execution of apoptosis. Surprisingly, in contexts not completely understood, the ripoptosome itself cleaves RIPK3, highlighting an apparent conundrum on how RIPK3 fulfills its role via the complex responsible for its own degradation. Recently, ripoptosome assembly was found to occur in mitosis where we found elevated RIPK3 levels. We now report that PLK1 directly associates with RIPK3 and phosphorylates it at S369 as cells enter mitosis. G2/M phase RIPK3 has pro-apoptotic activity but upon release from ripoptosome, can trigger necroptosis. Taken together, phosphorylation of RIPK3 at S369 prevents its ripoptosome-mediated cleavage thereby retaining its pro-death activity during mitosis.

## INTRODUCTION

Receptor-interacting protein kinase 3 plays a deterministic role in necroptosis—a form of regulated necrosis which is associated with a non-sterile, immunogenic response. RIPK3 is expressed ubiquitously and high levels of RIPK3 are associated with multiple major human pathological conditions including stroke-induced brain injury (Degterev et al., 2005, 2008), myocardial infarction (Luedde et al., 2014), atherosclerosis (Meng et al., 2016; Lin et al., 2013), aortic aneurysm (Wang et al., 2015; Wang et al., 2017), Gaucher's disease (Vitner et al., 2014), alcoholic liver disease (Roychowdhury et al., 2013), and toxic epidermal necrolysis (Choi et al., 2018) among others. In mouse models, RIPK3 loss protects against the forth mentioned diseases. More recently, the exclusively pro-necrotic role of RIPK3 has been challenged as it is found to participate in a more intricate signaling network where it can fulfill pro-apoptotic roles (Feoktistova et al., 2011; Tenev et al., 2011; Mandal et al., 2014). However, the molecular mechanisms responsible for switching between necroptosis and apoptosis remain incompletely understood. Studies of TNF receptor I-signaling suggest that necroptosis is triggered when Complex II—a protein-ensemble consisting of RIPK1, cFLIP(L), FADD and caspase 8—switches from a pro-apoptotic complex IIa (Micheau and Tschopp, 2003; Oberst et al., 2011) to a pro-necrotic complex IIb (Dondelinger et al., 2013). The inhibition of caspase 8 via pan-caspase inhibitors like zVAD-fmk (referred hereafter as zVAD) or its genetic ablation (Newton et al., 2014), coupled with the presence of RIPK3, is pivotal in switching complex II to a pro-necrotic complex that depends upon the kinase activity of RIPK1 and RIPK3. Unlike apoptosis which is activated by a cascade of proteolytic cleavage events, the execution of cell death by RIPK3 is regulated by several phosphorylation and de-phosphorylation events. Following the molecular events downstream of TNF-receptor I described above, RIPK3 associates with its partner RIPK1 through phosphorylation of S204 that promotes RIPK3 trans-autophosphorylation, culminating in RIPK3 T231 and S232 phosphorylation (Chen et al., 2013). RIPK3 phosphorylation is essential for its interaction with substrate MLKL whose activation results in plasma membrane rupture (Cai et al., 2014; Su et al., 2014; Wang et al., 2014; Sun et al., 2012). In contrast, the E3 ubiquitin ligase PPM1A degrades RIPK3 in a T182 phosphorylation-dependent manner (Choi et al., 2018), while Ppm1b-mediated de-phosphorylation of RIPK3 at S227 attenuates its necroptotic function (Chen et al., 2015). In agreement with phosphorylation dependent regulation of RIPK3's function, many residues are found to be phosphorylated on RIPK3 but their physiological role has not yet been described (Chen et al., 2013).

<sup>1</sup>Division of Vascular Surgery, Department of Surgery, University of Wisconsin-Madison, 1111 Highland Avenue, Madison, WI 53705, USA

<sup>2</sup>Department of Cell and Regenerative Biology, University of Wisconsin-Madison, Madison, WI, USA

<sup>3</sup>Lead contact

\*Correspondence: liub@surgery.wisc.edu  
<https://doi.org/10.1016/j.isci.2021.102320>



Under certain conditions, Complex IIa displays proteolytic activities via caspase 8 and is referred to as the ripoptosome in this context (Feoktistova et al., 2011; Tenev et al., 2011; Mandal et al., 2014). Surprisingly, the formation of ripoptosome does not appear to be dependent of TNF $\alpha$ -engagement. This ~2MDa complex is formed when cIAPs are inhibited (such as *in vitro* by using smac-mimetics), thereby releasing non-ubiquitinated RIPK1 which is suitable for bringing this multi-protein complex together (Tenev et al., 2011). Ripoptosome is generally subpar in executing apoptosis via caspase 8 processing, but by provoking small bursts of proteolytic activity of pro-caspase 8, ripoptosome cleaves RIPK3 and other substrates (Liccardi et al., 2019; Feng et al., 2007). It is believed that by cleaving RIPK3, ripoptosome ensures that spurious necroptosis is held in check<sup>15</sup>. Although assembly of the ripoptosome does not require RIPK3, a ripoptosome-like platform bound to RIPK3 has been demonstrated in some special contexts (Mandal et al., 2014). The attenuation of RIPK3 kinase activity via chemical inhibitors such as GSK'843 and GSK'872 (Mandal et al., 2014), or via mutations in its kinase site D161N (Newton et al., 2014), results in the assembly of ripoptosome that subsequently causes cell apoptosis via caspase 8. It is speculated that the conformation change of RIPK3 is responsible for its incorporation into a ripoptosome-like platform (Mandal et al., 2014; Newton et al., 2014). However, there is no unequivocal evidence that explains how RIPK3 resists the proteolytic activity of ripoptosome. Furthermore, in the presence of kinase inhibition, it is difficult to assess whether the ripoptosome-bound RIPK3 retains pro-necroptotic activity.

Recently, it was demonstrated that the ripoptosome forms physiologically during mitosis within which pro-caspase 8 is catalytically more active than in interphase cells. In the current report, we identify that RIPK3 is an additional component of the ripoptosome in G2/M phases and elicits increased apoptotic activity. We discover that PLK1-dependent RIPK3 phosphorylation leads to G2/M-specific accumulation and activity.

## RESULTS

### RIPK3 associates with the ripoptosome in the G2/M phases of the cell cycle

The physiological assembly of the ripoptosome during mitosis led us to ascertain the fate of RIPK3 over the course of the cell cycle. We used serum starvation and release to synchronize L929 cells. Serum starvation causes G0/G1-phase arrest and 10 h after addition of serum ~80% of the cells entered the G2/M phases (Figure S1A). RIPK3 was found to be the lowest in the G1 phase and became more abundant as the cell cycle advanced to the M phase (latter indicated by pH3S10—a marker of active mitosis) (Figure 1A). A similar pattern of cell-cycle-associated RIPK3 oscillation was observed in double-thymidine-based synchronized cells where a combination of elevated cyclin A levels in S, G2, and M phases, absence of cyclin D1 in S phase and H3S10-specific phosphorylation in mitosis indicates the accuracy of synchronization using these molecular markers of cell cycle (Figure S1B). Of note, RIPK1, whose association with RIPK3 is required by necroptosis of many cell types, remained constant throughout the cell cycle (Figure S1B). To better resolve G2 and M phases, we performed nocodazole chase experiment and found RIPK3 to be elevated in nocodazole arrested cells, indicating that RIPK3 protein is accumulated in mitosis, but not RIPK1 (Figure 1B). Notably, as cells enter the second round of mitosis, RIPK3 is concurrently elevated suggesting that RIPK3 levels are linked to G2/M phases and not artificial to the synchronization method. The differential accumulation of RIPK3 is not limited to mouse cells (Figure S1C). The cell-cycle-associated RIPK3 oscillation is at least in part intrinsic to the RIPK3 protein because exogenously expressed HA-tagged RIPK3 (HA-RIPK3) showed a similar accumulation kinetics (Figures 1C and S1D). We also found higher levels of RIPK3 mRNA in S and G2 as compared to the G1 phase (Figure S1E). Elevated ripoptosome activity during mitosis has been demonstrated in MEFs, among other cells. We observed that MEFs exhibited a RIPK3 oscillation pattern that was similar to what was observed in L929 cells. The levels of the other ripoptosome components, including FADD, RIPK1, and caspase 8, are shown; the necroptosis mediator RIPK1 remained constant throughout the cell cycle (Figure 1D). We focused on RIPK3 oscillation and examined the association of RIPK3 with ripoptosome. We disrupted the ripoptosome by silencing RIPK1 (a non-proteolytic component of the ripoptosome) and this led to increased RIPK3 level (Figure 1E), suggesting that disrupting the ripoptosome can elevate RIPK3 levels—an observation suggesting ripoptosome-mediated RIPK3 degradation. Next, we immunoprecipitated RIPK1 from serum-starved (G1 phase) cells and those released from serum (G2/M phase). Relative to G1 phase cells, exogenously expressed RIPK3 demonstrates increased association with the ripoptosome in G2/M phases. As expected, GSK'843 which is known to stimulate ripoptosome formation serves as positive control and increased RIPK3 association while disruption of the ripoptosome by adding Nec1s also prevents RIPK3 association (Figure 1F).

### RIPK3/rioptosome-mediated apoptosis occurs preferentially over RIPK3-independent apoptosis in actively cycling cells

Having detected increased RIPK3/rioptosome complexes in cells during G2/M, we postulated that relative to G1 arrested cells, actively dividing cells may display higher ripoptosome-dependent apoptosis over

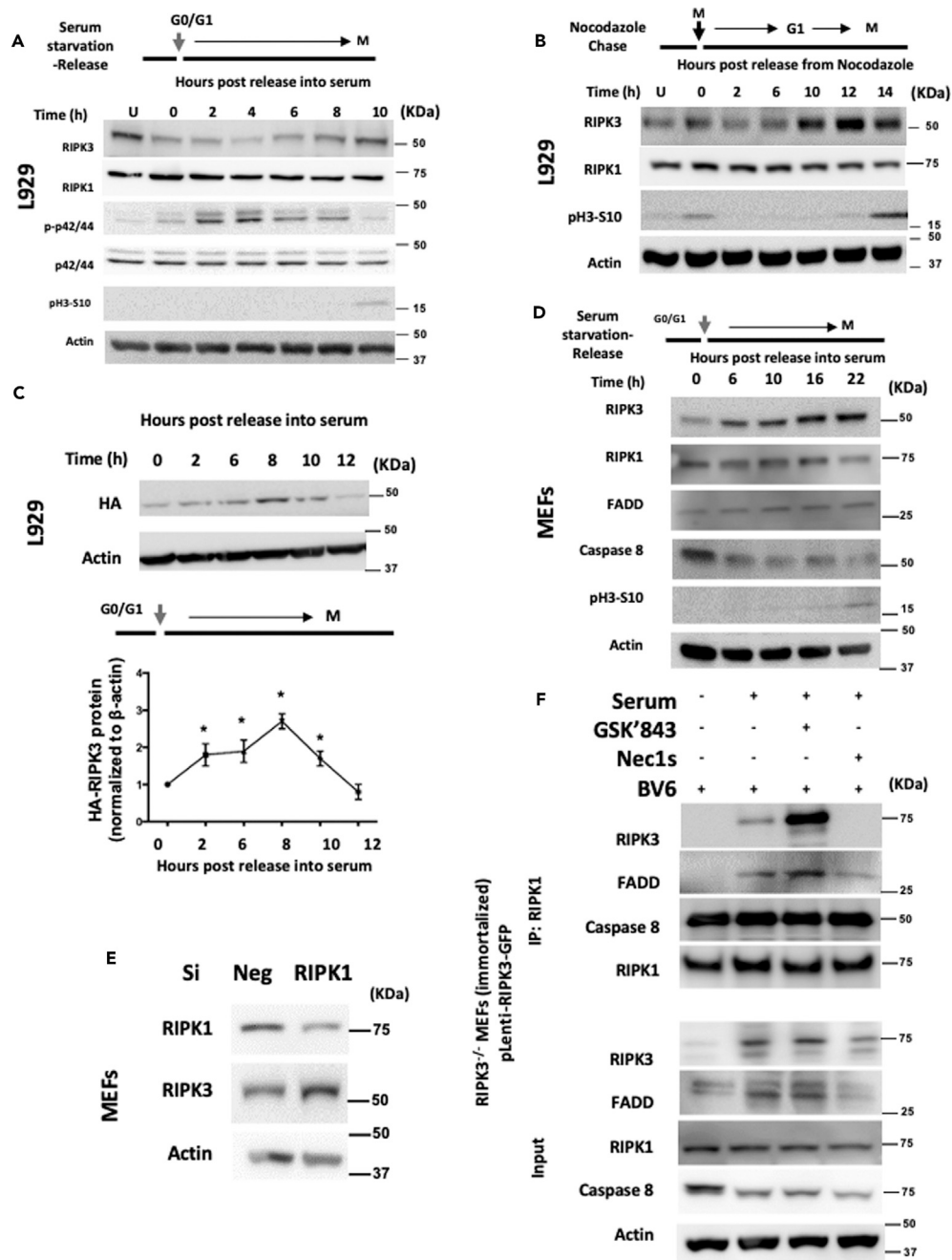


**Figure 1. RIPK3 is a component of the ripoptosome during G2/M phases**

(A) L929 cells were arrested by serum withdrawal for 36h. Indicated samples were released from serum by adding 10% (v/v) serum. Cells were lysed at various time points after serum restoration and analyzed by western blotting for RIPK3 protein levels. (U = no treatment was performed).

(B) L929 cells were treated with thymidine for 16h, released for 3h. 100 ng/mL nocodazole was added for an additional 10h and cells were released by addition of complete medium and harvested at indicated time points. Western blot analysis was performed in cells harvested at these time points.

(C) L929 cells were arrested by serum starvation for 36h and infected with adenoviruses encoding HA-RIPK3 (M.O.I of 1000) 12h after serum withdrawal. Cells were left arrested (G0/G1-phase) or released for indicated times after which the cells were lysed and RIPK3 levels were analyzed using western blotting.

(D) RIPK3 expressing primary MEFs were synchronized by serum starvation and released for indicated times by the addition of 10% serum. Cells were harvested and proteins were analyzed by western blotting against indicated proteins.

**Figure 1. Continued**

(E) *Ripk3*<sup>+/+</sup> MEFs were transfected with siRNA against non-specific target (siNeg) or RIPK1 (siRIPK1). 3h prior to harvest, 10  $\mu$ M BV6 was added. Cell-lysates were prepared 36h post-transfection and analyzed by western blotting.  
(F) Immortalized *Ripk3*<sup>-/-</sup> MEFs transduced with RIPK3-GFP were synchronized using serum starvation and release. Released cells were treated with 10  $\mu$ M BV6 and 10  $\mu$ M GSK'843 or Nec1s (1  $\mu$ M). Immunoprecipitation was performed using RIPK1 antibody and analyzed using indicated antibodies \*p < 0.05 analyzed by one-way ANOVA.

RIPK3-independent apoptosis (Figure 2A). To test whether increased ripoptosome formation impacts apoptosis in G2/M via RIPK3, we treated serum-starved or released *Ripk3*<sup>+/+</sup> MEFs with the RIPK3 kinase inhibitors GSK'843 or GSK'872 that are known to causes apoptosis in a ripoptosome-dependent manner (Mandal et al., 2014). Indeed, GSK'843 and GSK'872 induced greater apoptosis in actively cycling cells than the cells that remained arrested (Figures 2B, 2C, and S2). The elevated apoptotic events were blunted by zVAD or in *Ripk3*<sup>-/-</sup> MEFs, confirming the ripoptosome-dependent apoptosis mode. Consistently, GSK'872-challenged G2/M wild type (WT) cells showed higher levels of cleavage of caspase 3 than the challenged G1 cells (Figure 2D). Cleaved caspase 3 was not detected in *Ripk3*<sup>-/-</sup> MEFs (Figure 2D), highlighting the necessity of RIPK3 in this process. In contrast, staurosporine caused apoptosis in serum-starved cells but not in actively cycling cells (Figure 2E). Furthermore, staurosporine caused caspase 3 cleavage in serum-starved cells regardless of their *Ripk3* genotype (Figure 2F). These data demonstrate that RIPK3 is critical for ripoptosome-mediated apoptosis during G2/M, where the ability to undergo RIPK3-independent intrinsic apoptosis is diminished.

**RIPK3 retains its pro-necrotic kinase activity in the G2/M phases but is restrained by the ripoptosome**

Next, we evaluated cell-sensitivity to necroptosis during the cell cycle. Toward this, we subjected synchronized L929 cells to TNF $\alpha$  stimulation in the presence of zVAD. Shown in Figure 3A, G0/G1-arrested cells were markedly insensitivity to necroptosis induction compared to cells at the G2/M phase, reflected by lower uptake of propidium iodide (PI). Flow cytometry analysis confirmed that G0/G1-arrested cells were more resistant to necroptosis compared to non-synchronized cells, whereas cells in the G2/M phase were most responsive to necroptosis induction (Figure 3B). The kinetics of necroptosis resembled that of RIPK3 oscillation (Figure S3A). The divergent sensitivity toward necroptosis was also observed when cells were synchronized by double-thymidine block and subsequent release (Figure S3B). In agreement with the necroptosis sensitivity, TNF $\alpha$  -induced RIPK3-RIPK1 association was found to be higher at G2/M phase compared to G1 phase (Figure 3C) when cells are undergoing necroptosis (indicated by pMLKL). At the level of cell-death, the enhanced necrotic response at the G2/M phase was absent in *Ripk3*<sup>-/-</sup> MEF or siRIPK3 L929 cells (Figures 3D, 3E, and S3C) confirming that RIPK3 underlies the cell cycle-specific necroptotic response. Consistent with the necroptosis literature, TNF $\alpha$  caused heightened necrosis only under conditions where caspase 8 was inhibited by the pan-caspase inhibitor zVAD (Figure 3F) or by shRNA (Figure 3G). These data suggest that higher RIPK3 during G2/M enables higher sensitivity to necroptosis stimuli during cell division but disrupting caspase 8 is essential to free RIPK3 for necroptosis.

**PLK1 is necessary for RIPK3 accumulation**

One potential explanation for the high RIPK3 accumulation in the G2/M phase despite of its association with the ripoptosome is an acquired resistance to proteolysis via post-translational modification. An analysis of the RIPK3 amino acid sequence using eukaryotic linear motif resource revealed several consensus sites for post-translational modifications that are conserved across species (Table S1). The predicted sites included those for cyclin dependent kinase 1 (CDK1), GSK3 $\beta$ , casein kinase 1 (CK1), APC/C, and Polo-like kinase 1 (PLK1). Using known inhibitors to these kinases or ubiquitin ligase (APC/C), we probed the role of these kinases in RIPK3 accumulation. BI2536, an inhibitor of Polo-like kinase, caused a robust reduction in RIPK3 levels without affecting cell cycle progression at this concentration (Figures 4A and S4B). Other inhibitors did not appear to affect RIPK3 levels (Figure S4A). Knocking down PLK1 phenocopied the effect of BI2536 on RIPK3 (Figure 4B) but did not appear to alter other ripoptosome-proteins significantly. The effect of PLK1 silencing was also true in A375 cells that expressed a doxycycline inducible shRNA for non-targeting control (shCtr) or PLK1 (shPLK1) (Figure S4C). Based on different approaches to abrogate PLK1, we concluded that RIPK3 levels are linked to PLK1. We then immunoprecipitated RIPK3 in cells in G1/S or G2/M phases and found PLK1 to be enriched in mitosis in the IP fraction but not in isotype control (Figures 4C, S4D, and S4E). The amount of PLK1 in the IP fraction appeared to be independent of the inhibitor BI2536 suggesting that PLK1 activity is independent from its physical interaction with RIPK3. The

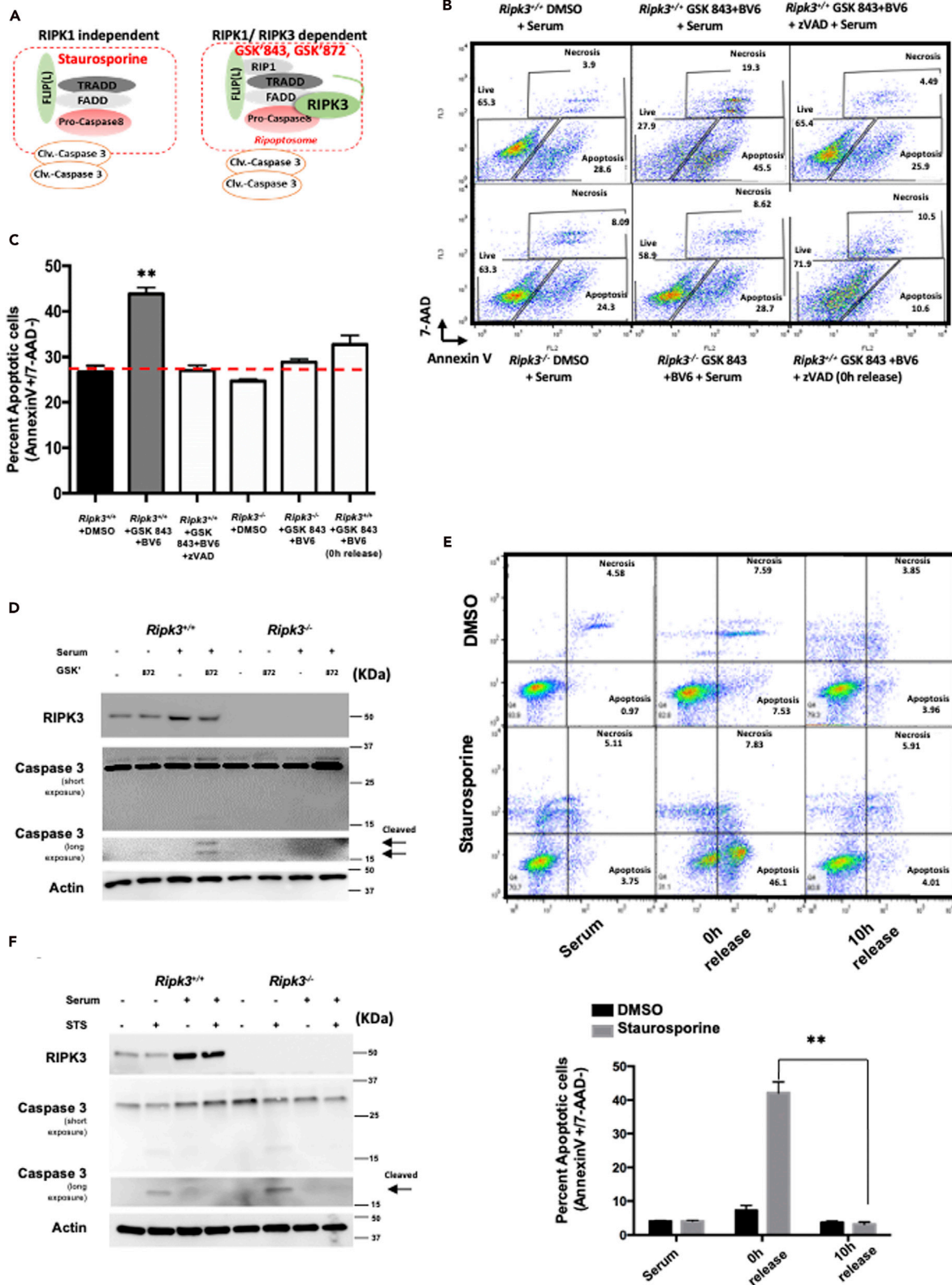


**Figure 2. G2/M phases are associated with increased RIPK3-mediated apoptosis**

(A) Schematic representation of RIPK3 independent and dependent apoptosis inducing complex. (B and C) *Ripk3*<sup>+/+</sup> or *Ripk3*<sup>-/-</sup> MEFs were synchronized by serum starvation and released for 16h by the addition of 10% serum. 3h before harvesting cells, 10  $\mu$ M GSK'843 was added along with 20  $\mu$ M zVAD and 10  $\mu$ M BV6 where indicated. Cell death was evaluated by flow cytometry (B). Bar graph shows percent apoptosis (Annexin V+/7-AAD-) (C). (D) *Ripk3*<sup>+/+</sup> or *Ripk3*<sup>-/-</sup> MEFs were synchronized by serum starvation and released for 16h by adding 10% (v/v) of serum. 10  $\mu$ M GSK'872 and 10  $\mu$ M BV6 were added 2h before harvesting cells for western blotting with indicated antibodies. (E and F) Synchronized cells were treated with DMSO or 1  $\mu$ M staurosporine (STS) for 2h before harvesting and analyzed by flow cytometry (E) or western blotting (F). All data shown are mean  $\pm$  SD of three or more independent experiments. Flow cytometry data is representative of mean  $\pm$  SD of triplicates from one experiment repeated three times with consistent results. \*\*p < 0.01 using two-way ANOVA.

predicted PLK1 consensus site locates in the proline-rich domain (PRD) of RIPK3 that is outside of its kinase domain (KD). To identify the region of interaction, we cloned and expressed various domains of RIPK3 fused with Myc, including full-length (FL), KD, non-kinase domain (NKD) and PRD (Figure 4D). HEK293T cells were co-transfected with equal amounts of PLK1-FLAG along with various domains of myc-tagged RIPK3, followed by co-immunoprecipitation using an anti-myc antibody. The FL, NKD, and PRD (each containing the putative PLK1 consensus site) were able to pull-down PLK1-FLAG, but not the KD or myc-tag alone (Figure 4E), strongly favoring the idea that RIPK3 interacts with PLK1 through the predicted PLK1 binding site. Next, we ascertained whether RIPK3 and PLK1 co-localize during various cell-cycle phases by measuring the extent of overlap between RIPK3 and PLK1 using confocal microscopy. A trend toward increased co-localization in mitosis relative to interphase cells was observed as demonstrated by the Pearson coefficient (Figure 4F). In addition, we utilized proximity ligation assay to assess the PLK1/RIPK3 complexes in interphase and the mitotic phases in asynchronous cells. We observed that PLK1/RIPK3 complexes, demonstrated by punctae, were abundant in the prophase and metaphase and sporadic in the anaphase and telophase, whereas very few punctae were observed in interphase cells (Figure 4G). As controls, samples with no RIPK3 primary antibody were used and no significant background (punctae) was observed (data not shown). This data agree with the known degradation of PLK1 during the metaphase to anaphase transition.

**PLK1 phosphorylates RIPK3 at S369**

To test whether PLK1 phosphorylates RIPK3, we incubated recombinant PLK1 and RIPK3 in the presence or absence of BI2536. PLK1 caused Serine phosphorylation on RIPK3, which was diminished by the addition of BI2536 (Figure 5A). Next, we immunoprecipitated RIPK3 from L929 cells that were released from serum starvation (for 10h) in the presence of DMSO or BI2536 (Figure 5B). Mass spectrometry was performed on the samples and S369 phospho-peptide was found to be strongly enriched in DMSO-treated G2/M IP fraction but not in the BI2536-treated G2/M samples or G1/S (DMSO- or BI2536-treated) samples (Figures 5C and S5A). This G2/M-specific decrease in response to BI2536 was also observed when with exogenously expressed RIPK3-eGFP, reinforcing the idea that PLK1 promotes RIPK3 accumulation at the level of protein stability (Figure 5D). We next examined whether overexpression of PLK1 boosts RIPK3 accumulation in G0/G1-arrested cells in a gain-of-function approach. We transfected FLAG-tagged PLK1 expressing constructs in MEFs that were either arrested by serum starvation or released into serum. We found that PLK1 overexpression increased RIPK3 levels in serum-arrested cells to a level that was comparable to the serum-stimulated cells (Figure 5E), indicating that exogenous PLK1 is sufficient to stabilize RIPK3 even in the G0/G1 cells. Next, we mutated the putative PLK1 consensus site within RIPK3 by substituting S369 or T368 with an alanine (hereafter RIPK3-PLK1 mutants). The lentiviruses that express GFP conjugated WT or RIPK3-PLK1 mutants including single or double mutations (T368A, S369A, and T368A S369A) were introduced to *Ripk3*<sup>-/-</sup> MEFs that were immortalized using SV40 large T antigen (LTA-MEFs). SV40 large T antigen itself did not alter the cell cycle-dependent RIPK3 oscillation (Figure S5B). Relative to WT, disruption of S369, T368 or both resulted in degradation of RIPK3 (Figure S5C) even in an unsynchronized population of the respective cell lines. Importantly, expression of RIPK3 WT or single mutants did not significantly alter cell death relative to *Ripk3*<sup>-/-</sup> cells (Figure S5D). We reasoned that if PLK1 directly acts on RIPK3 via T368 and/or S369, mutating these residues would prevent RIPK3 from responding to PLK1 overexpression. To this end we expressed PLK1 in MEFs expressing RIPK3-PLK1 mutants. Indeed, PLK1 overexpression enhanced the accumulation of WT RIPK3 but not T368A or RIPK3 S369A mutants (Figure 5F). Taken together, our loss and gain of function data strongly suggest that PLK1 stabilizes RIPK3 by phosphorylating RIPK3 at S369.

**RIPK3 S369 phosphorylation prevents ripoptosome-mediated cleavage of RIPK3**

Ripoptosome cleaves its substrates via the catalytic activity of caspase 8. We noticed that the caspase 8 site on RIPK3 (D333) lies ~36 amino acids away from the PLK1 phosphorylation site at S369 (Figure 6A) D333 site

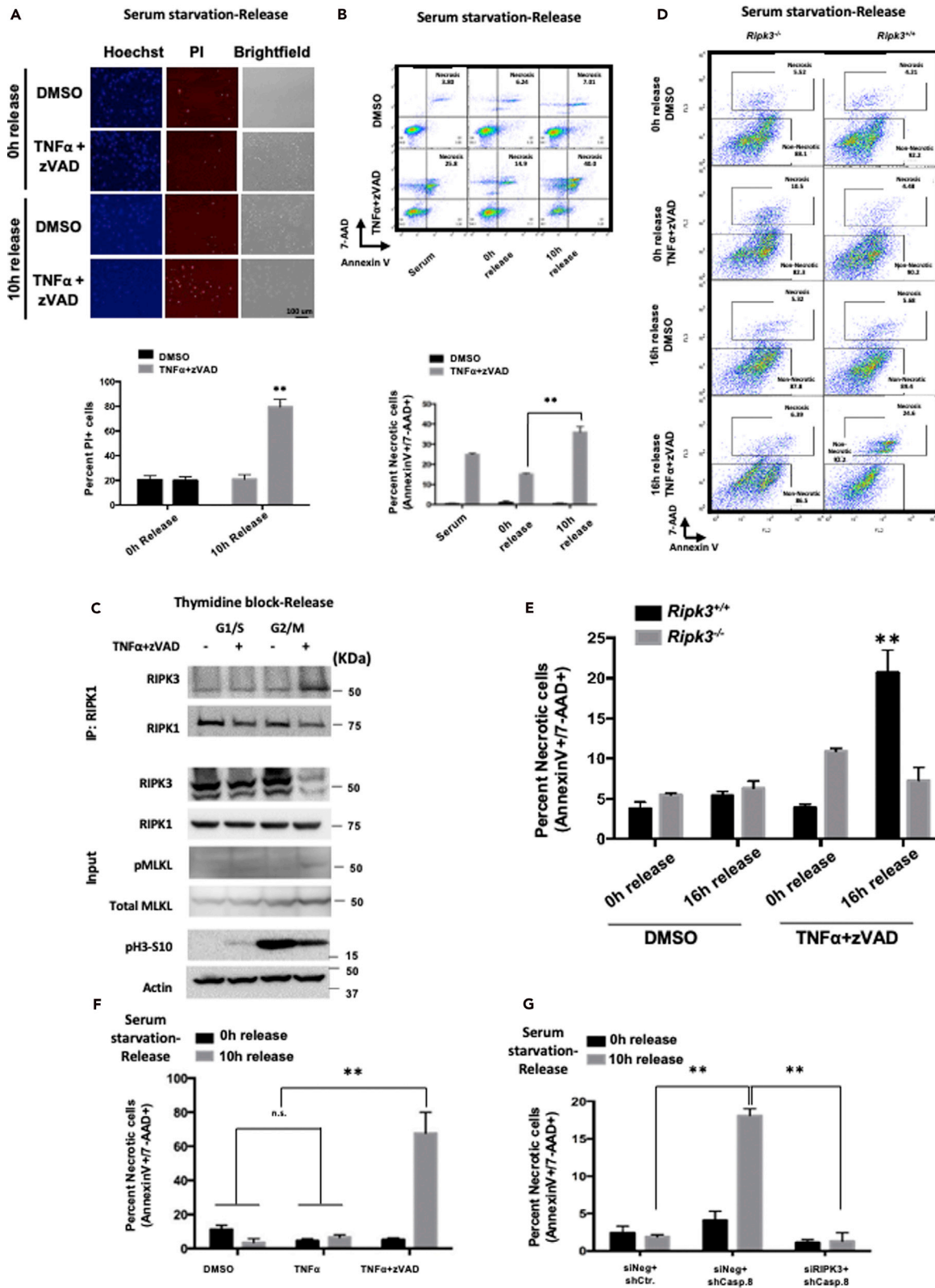


**Figure 3. RIPK3 is restrained inside the ripoptosome but retains its pro-necrotic kinase activity**

(A) L929 cells were seeded on glass slides. After cell attachment, serum was withdrawn for 36h and added back to a final concentration of 10% (v/v) in the indicated wells for 10h, followed by DMSO or 10 ng/mL TNF $\alpha$  and 20  $\mu$ M zVAD treatment for an additional 2h. Cells were then stained with Hoechst and propidium iodide (PI). Microscopic images were taken from 5 fields per well and evaluated for PI+ cells. Bar graph shows percent of cells positive for PI.

(B) L929 cells were left unsynchronized (serum), serum starved for 36h (0h release), or released from serum starvation for 10h by addition of 10% (v/v) of serum (10h release). After treatment with DMSO or 10 ng/mL TNF $\alpha$  +20  $\mu$ M zVAD for 2h, cells were harvested for flow cytometry analysis. The bar graph shows the percent necrotic cells.

(C) L929 cells were synchronized by double-thymidine block and treated with DMSO or 10 ng/mL TNF $\alpha$  +20  $\mu$ M zVAD for 2h before harvesting. Co-immunoprecipitation was performed using an anti-RIPK1 antibody followed by western blotting with indicated antibodies.

(D and E) *Ripk3*<sup>+/+</sup> or *Ripk3*<sup>-/-</sup> MEFs were synchronized by serum starvation and released for 16h by the addition of 10% serum. 4h before harvesting cells, DMSO or 50 ng/mL TNF $\alpha$ , 40  $\mu$ M zVAD and 10  $\mu$ M BV6 were added and cells were harvested for flow cytometry (D). Bar graph indicates percent necrosis (Annexin V+/7-AAD+) (E).

(F) L929 cells were serum starved for 36h and indicated samples were released by the addition of 10% (v/v) serum for 10h. Cells were treated with DMSO, 10ng/mL TNF $\alpha$  or 10ng/mL TNF $\alpha$  +20  $\mu$ M zVAD 2h before harvesting the cells. Annexin V/7-AAD based flow cytometry analysis was performed. Bar graph shows percent necrotic cells.

(G) L929 cells were withdrawn from serum and simultaneously infected with lentiviruses encoding the indicated shRNA and siRNAs for 36h. Cells were then released into serum for 10h and were harvested for Annexin V/7-AAD based flow cytometry. All data shown are mean  $\pm$  SD of three or more independent experiments. Flow cytometry data are representative of mean  $\pm$  SD of triplicates from one experiment repeated three times with consistent results. \*\*p < 0.01 using two-way ANOVA.

is nearly identical to the known caspase 8 cleavage site on human RIPK3 (Figure 6B) and based on this well conserved nature, we tested whether S369 phosphorylation antagonizes ripoptosome-mediated degradation via this caspase 8 cleavage site<sup>25</sup>. To test the role of caspase 8, we silenced caspase 8 in L929 cells (Figure 6C) and in *Ripk3*<sup>-/-</sup> MEFs expressing RIPK3-eGFP exogenously (Figure 6D). Silencing caspase 8 increased RIPK3 protein levels (Figures 6C and 6D). The increase in RIPK3 in caspase 8 silenced cells was specific to actively cycling cells, which is in agreement with the ripoptosome assembly during mitosis (Figures 6C and S6). Figures 6C and S6 also demonstrate that caspases such as caspase 3 and 9 remained unaffected by caspase 8 silencing or RIPK3 deficiency. To test whether RIPK3's recruitment in ripoptosome is dependent on the T368/S369 during G2/M in a caspase-sensitive manner, we immunoprecipitated FADD to isolate the ripoptosome in cells arrested in serum or released into serum for 16 hr (Figure 6E). As expected, the serum-starved cells had sparse levels of RIPK3 and ripoptosome, whereas only WT RIPK3 was enriched inside the ripoptosome in the actively cycling cells. RIPK3-*PLK1* mutants could only conditionally be rescued when zVAD was present (Figure 6E). In a complimentary gain-of-function approach, we generated a phosphomimetic version of RIPK3 S369 by substituting with serine with aspartic acid (i.e. S369D). We measured the incorporation of these RIPK3 mutants expressed in *Ripk3*<sup>-/-</sup> cells into the ripoptosome and found that the relative to eGFP and S369A mutant of RIPK3, S369D was protected from ripoptosome-mediated degradation (Figure 6F). To further demonstrate the interaction between D333 and S369 within the RIPK3 molecule, we generated a caspase-resistant mutant of RIPK3 (D333A) and determined whether the D333A mutation rescues a non-phosphorylatable version of RIPK3 (T368A S369A) from degradation. In *Ripk3*<sup>-/-</sup> LTA MEFs, we exogenously expressed the indicated versions of RIPK3-eGFP. In support of our hypothesis, we first notice the dramatic stability of RIPK3 D333, validating the involvement if this site in RIPK3 stability. Further, loss of phosphorylation mutant (TS >> AA) diminished RIPK3 expression which was rescued by an accompanying mutation in the caspase 8 dead site (Figure 6G). These data demonstrate that RIPK3 T368S369 is essential for the incorporation of RIPK3 into the ripoptosome, likely via resisting caspase-cleavage at a proximal site (Figure 6H).

**DISCUSSION**

Since the initial discovery of RIPK3 and its critical involvement in executing necroptosis, several independent reports have demonstrated that RIPK3 may trigger apoptosis through a unique pathway distinct from the classically defined apoptosis pathway (Mandal et al., 2014)(Newton et al., 2014). Extending from the recent report by Liccardi et al. that ripoptosome is assembled physiologically during mitosis<sup>24</sup>, we showed that the levels of RIPK3 oscillated during the cell cycle. Cells in the G2/M phases contained higher levels of RIPK3 than cells in the G1 phase. Furthermore, data from the co-immunoprecipitation analysis indicated greater association between RIPK3 and ripoptosome in the G2/M than G1 phase. These new findings are significant in multiple aspects. To the best of our knowledge, this is the first demonstration that intracellular levels of RIPK3 are not constant. We speculate that the cell-cycle-associated variation in RIPK3 content may confer cells with different sensitivity (or resistance) to cell death. It has been known that G2/M cells are relatively resistant to apoptosis than G1 cells (Castedo et al., 2004; Pucci et al., 2000; Altieri, 2003). Here, we report a temporal pattern of necroptosis sensitivity that compliments that of apoptosis. It is not

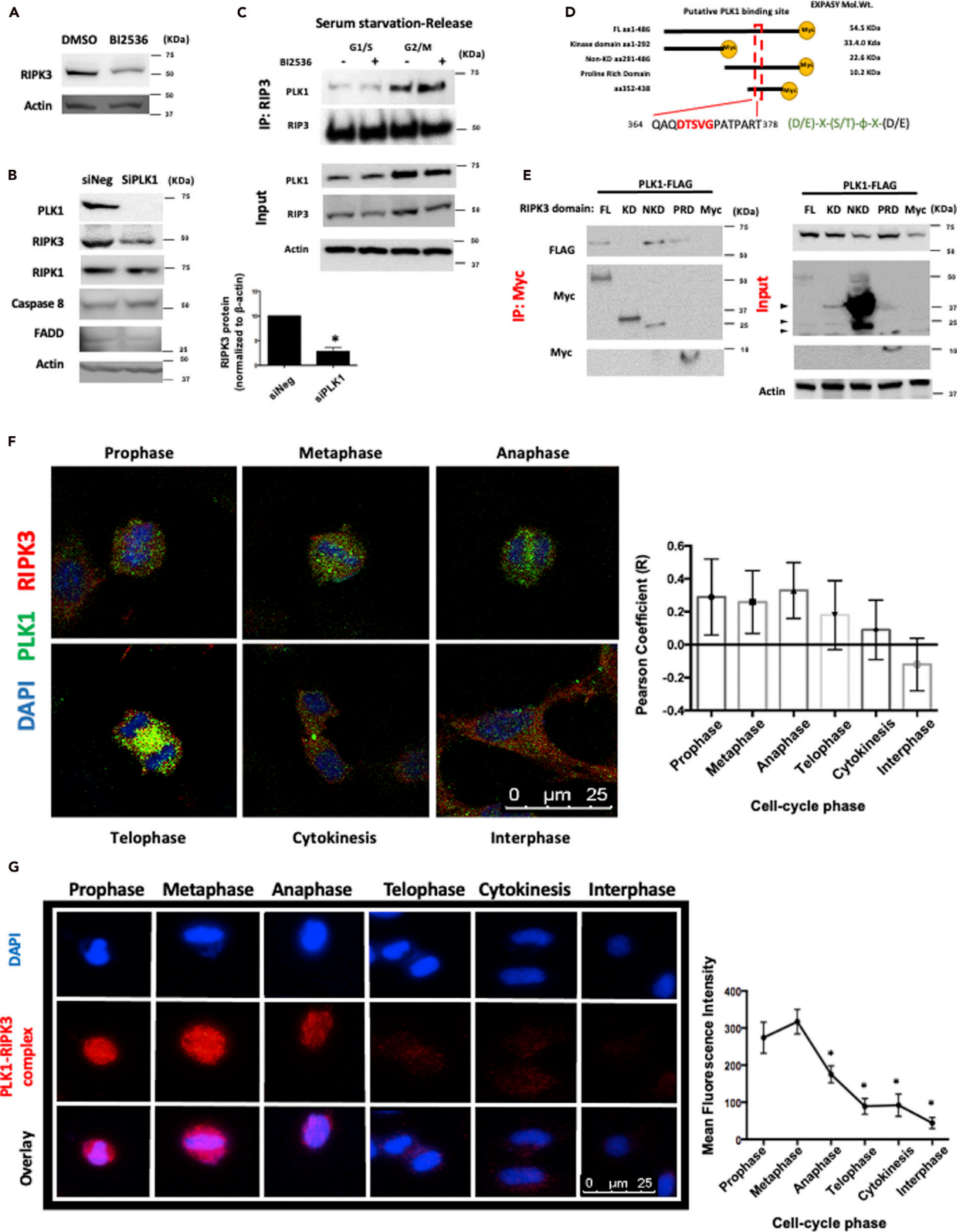


**Figure 4. PLK1 activity is essential for RIPK3 stability**

(A) L929 cells were treated with DMSO or BI2536 (10nM) and harvested 36h later for western blotting.  
 (B) siRNA against non-targeting control (siNeg) or PLK1 (siPLK1) was transfected in L929 cells. 36h after siRNA treatment, cell lysates were analyzed by western blotting. RIPK3 levels were normalized to beta-actin and were quantified relative to siNeg.  
 (C) L929 cells were synchronized by serum starvation and released and 10 nM BI2536 was added at release in indicated samples. IP was performed using RIPK3 antibody and immunoprecipitated proteins were analyzed using indicated antibodies.  
 (D) Schematic overview of the C-terminal Myc-tagged domains of RIPK3 used in E and their molecular weights calculated using ExPASy molecular weight tool.  
 (E) 293T cells were co-transfected with C-terminal PLK1-FLAG and a Myc-tagged RIPK3 domain. Co-immunoprecipitation was performed using an anti-Myc antibody. Western blotting was used to analyze proteins in the input and the IP fraction. Arrowheads indicate non-specific bands.  
 (F) Unsynchronized L929 cells were cultured on glass slides and confocal microscopy was performed using PLK1 (green, Alexa 488) and RIPK3 (red, Alexa 594), followed by staining with DAPI immediately before mounting. Cells were identified in the various phases based on the nuclear-morphology.  
 (G) Representative images of proximity ligation assay (PLA) performed for PLK1 and RIPK3. Unsynchronized L929 cells were cultured on glass slides and PLA was performed using PLK1 (mouse antibody) and RIPK3 (rabbit antibody), followed by staining with DAPI immediately before mounting. Cells were identified in the various phases based on the nuclear morphology. Mean fluorescence intensity was quantified per cell and shown in the graph. All data shown are mean  $\pm$  SD of three or more independent experiments. Flow cytometry data are representative of mean  $\pm$  SD of triplicates from one experiment repeated three times with consistent results. \* $p < 0.05$  using Student's t-test (B), two-way ANOVA (C) or one-way ANOVA (G). Arrowheads represent non-specific bands.

entirely clear as to why the RIPK3-independent apoptosis machinery is dismantled during G2/M phases of the cell cycle. Caspase 3 (Shin et al., 2001), 7 (Shin et al., 2001), 8 (Matthess et al., 2014) and 9 (Allan and Clarke, 2007) and other critical cell-death modulators are inhibited during mitosis through mechanisms such as post-translational modifications or via G2/M restricted apoptosis-inhibiting proteins such as survivin. Perhaps, elevated RIPK3 in G2/M provides cells an alternative to die if a mitosis error shall occur.

Our finding of concurrent elevation of RIPK3 protein accumulation and its ripoptosome association presents an apparent paradox. We used multiple genetic, molecular and pharmacological approaches to address how RIPK3 accumulates at G2/M when the ripoptosome is also present. Our data suggest that both transcriptional and posttranslational mechanisms underlie RIPK3 accumulation. In part, the oscillation is due to increased mRNA synthesis of RIPK3 in S and G2 phases owing to the presence of the CDE and CHR elements (Badie et al., 2000; Muller et al., 2017) and partly via protein stability. We focused on phosphorylation and identified serine 369 phosphorylation by PLK1 as a mechanism underlying RIPK3's accumulation during G2/M. Inhibition of PLK1 abolished RIPK3 accumulation and S369 phosphorylation. Furthermore, the loss of function mutagenesis of serine 369 (S369A) replicated the effect of PLK1 inhibition while a phosphorylation mimic mutation (S369D) increased RIPK3 accumulation. The identification of this phosphorylation site is supported by a previous mass spectrometry experiment in NIH-3T3A cells where exogenous FLAG-RIPK3 was found to bear several phosphorylations including S369 (Chen et al., 2013). However, no kinase or mechanistic function of this phosphorylation had been previously reported. Thus, our identification of PLK1-mediated phosphorylation advances RIPK3 biology. Literature has established phosphorylation to be a critical step for activation of RIPK3's pro-necrotic activity. Phosphorylation at serine 204 by RIPK1 (McQuade et al., 2013) and autophosphorylation of RIPK3 at T231 and S232 (Chen et al., 2013) are necessary events to induce necroptosis. We do not currently know whether S369 phosphorylation affects the kinase activity of RIPK3. However, disruption of this phosphorylation decreased RIPK3 protein content, suggesting this site regulates RIPK3 protein stability. PLK1 may not be the only kinase responsible for S369 phosphorylation. However, PLK1 has been known to be abundantly present in G2/M phase (Eckerdt and Strebhardt, 2006) (Lindon and Pines, 2004; van de Weerd et al., 2005). Liccardi et al. recently found PLK1 in ripoptosome in these phases, suggesting that PLK1 is in the proximity of RIPK3 within G2/M cells, which supports the feasibility of our proposed phosphorylation. Notably, our mass spectrometry data indicates that the S369 phosphorylation is attenuated in G2/M phases upon PLK1 inhibition. Given the G2/M restricted expression of PLK1, we speculate that this phosphorylation occurs during these phases of the cell cycle.

RIPK3 is demonstrated to be degraded by the proteolytic activity within ripoptosome, namely caspase 8. Multiple lines of data demonstrate that S369 phosphorylation prevents ripoptosome from degrading RIPK3, likely by direct inhibition of caspase-mediated cleavage. First, disruption of S369 leads to spontaneous degradation of RIPK3 which can be rescued by a cis-mutation that abrogates the caspase-cleavage site (D333). Second, the phosphomimetic S369D mutant resists spontaneous degradation. Lastly, S369D mutant can be found associated with the ripoptosome using co-IP, whereas S369A cannot be found in this complex. Together, these data suggest that S369 phosphorylation is essential for RIPK3 stability by

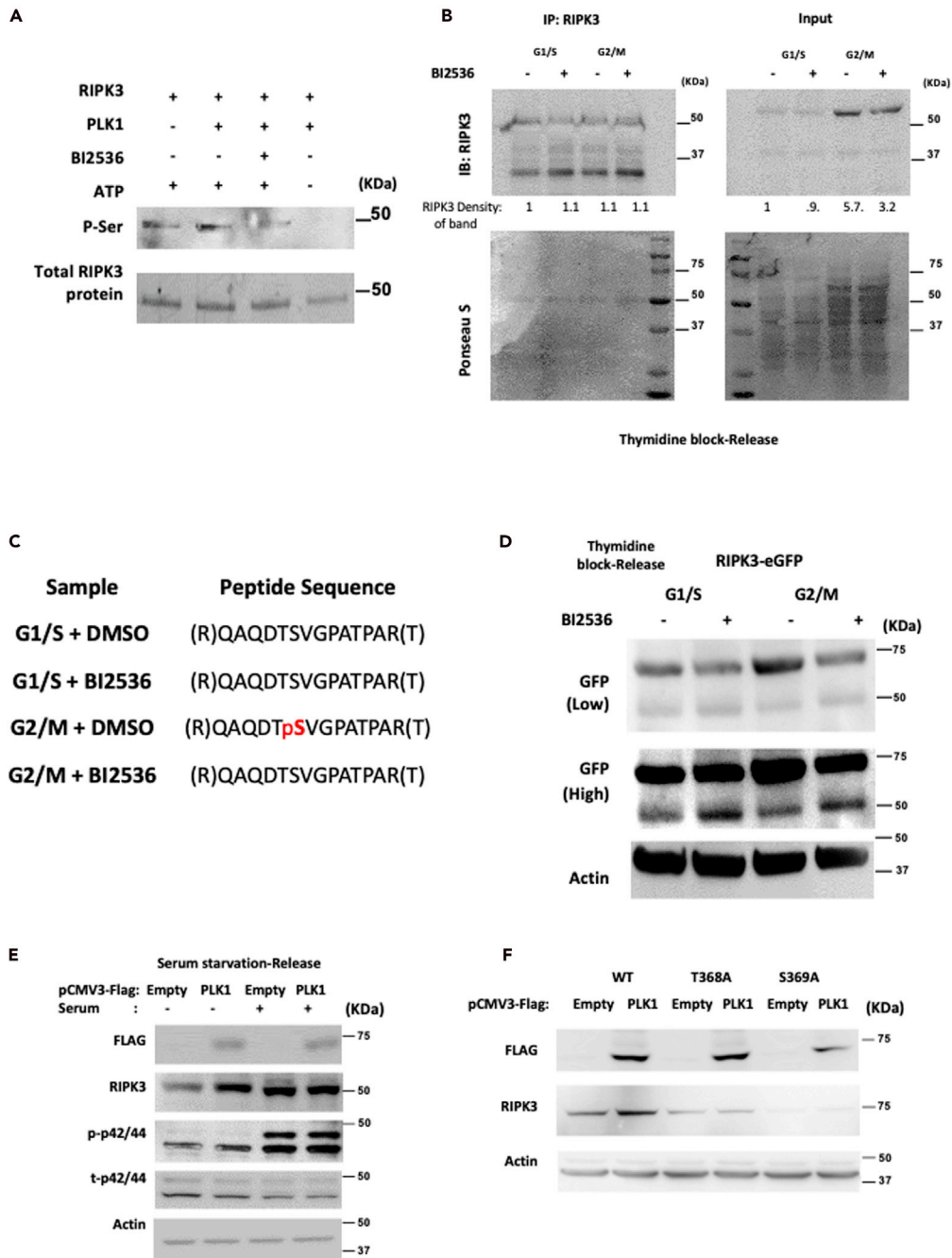


**Figure 5. S369 phosphorylation by PLK1 is necessary for RIPK3 stability**

(A) Recombinant mouse PLK1 and RIPK3 were incubated at 30°C in the presence or absence of ATP for 1 h. The protein mixture was blotted with an anti-phosphorylated serine antibody. PLK1 inhibitor BI2536 was included to demonstrate PLK1-dependence. Total RIPK3 protein was measured using TGX-Stain-Free gels® (see [methods](#)) to demonstrate equal amounts of substrate used in different reactions.

(B and C) Cells were synchronized by double-thymidine block and treated with DMSO or BI2536. To analyze RIPK3 protein modifications by mass spectrometry, RIPK3 protein was isolated using IP. The immunoprecipitated product was analyzed by western blotting to ensure RIPK3 is indeed enriched (B) and subsequently deposited for mass spectrometry. Peptides corresponding to the putative phosphorylation site are depicted (C).

(D) Cells were transfected with RIPK3-eGFP expressing construct and synchronized using double-thymidine block. After release for 8h from the second thymidine block, samples were analyzed by western blotting.

**Figure 5. Continued**

(E) Mouse embryonic fibroblasts (MEFs) were seeded and after cell attachment, serum was withdrawn. After 24h, cells were transfected with pCMV3-PLK1-FLAG expressing construct or pCMV3 vector construct for an additional 12h. Indicated samples were then treated with 10% (v/v) serum for 10h. Samples were analyzed by western blotting for indicated proteins.

(F) *Ripk3*<sup>-/-</sup> LTA-MEFs were infected with lentiviruses encoding RIPK3-GFP (WT) or the indicated amino acid substitutions. Cell lines with the indicated substitutions were transfected with pCMV3-PLK1-FLAG expressing construct or pCMV3 vector construct (empty) for 36h and cells were harvested for western blotting.

preventing caspase 8 from cleaving it. Since the ripoptosome is a large, ~2 MDa complex, it is currently unclear whether this complex spans the 36 amino acids between S369 and D333, or whether the antagonism is dependent on the spatial conformation of RIPK3 and the ripoptosome.

Our data provide new mechanistic insight into RIPK3 biology, where its conformation has loosely been associated with its apoptotic versus necroptotic propensity (Mandal et al., 2014; Newton et al., 2014). Previously, inhibition of RIPK3's kinase activity via GSK'872 and GSK'843 has been found to elicit RIPK3-dependent apoptosis (Mandal et al., 2014). Our co-IP data on G2/M phase cells revealed physiological association of RIPK3 with ripoptosome (independent of GSK'872 and GSK'843) suggesting that the known conformation "modifiers" of RIPK3 are not obligatory for its stability in the G2/M phases of the cell cycle. In fact, depending on the stimulus used, G2/M phase RIPK3 can be shunted into RIPK3-dependent apoptosis, as well as necroptosis. However, caspase 8 inhibition or silencing is required for G2/M phase necroptosis, likely to free RIPK3 from the ripoptosome. This idea is also supported by our finding that RIPK3 levels incremented upon RIPK1 silencing. To this end, S369 phosphorylation of RIPK3 is essential for this plasticity.

In light of the technical differences in cell-synchronization by Liccardi et al. (mitotic "shake-off" versus serum release) and the challenge in capturing the transient mitotic population, it may be argued that observed increment in RIPK3 levels and its functions are limited to the G2 phase but not during mitosis when the ripoptosome complex is assembled. Toward this, we observed increased necroptosis in nocodazole arrested cells which represent a mitotic population, demonstrating that necroptosis is elevated in mitosis. Further, we observe greater PLK1-RIPK3 complexes in proximity ligation assay (as also demonstrated by the Liccardi et al.) relative to interphase cells, again suggesting that RIPK3 is present in mitosis although PLA does not indicate absolute amounts. Lastly, Frank et al. demonstrate increased interferon induced necroptosis specifically in mitosis (Frank et al., 2019) suggesting that RIPK3 is present adequately and also promotes this RIPK1-independent form of necroptosis. These data suggest that RIPK3 is protected from increased caspase 8 activity during mitosis, likely until anaphase.

In summary, our findings fill a knowledge gap in how G2/M phases of the cell cycle have elevated RIPK3 protein in spite of ripoptosome formation. We demonstrate that RIPK3 in the G2/M phases physiologically associates with the ripoptosome. Relative to G1 and S-phases, RIPK3 expressed in G2/M phase elicits increased apoptosis when cells are treated with pro-apoptotic chemicals GSK'872 and GSK'843. However, RIPK3 may be shunted into necroptosis when caspase 8 is silenced or inhibited by zVAD during G2/M phases. Mechanistically, our data indicate PLK1-mediated phosphorylation at S369 underlies RIPK3 stability within the ripoptosome complex. RIPK3 phosphorylation at S369 confers resistance to ripoptosome-mediated cleavage, allowing RIPK3 to perform its function within the ripoptosome to trigger apoptosis, and outside the ripoptosome to trigger necroptosis. Our findings are the first to demonstrate the prominence of RIPK3-mediated apoptosis in actively cycling cells and the shift toward RIPK3 may have evolved as a mechanism by which the responsibility of balancing necroptosis vs apoptosis in mitotic cells converges on RIPK3.

**Limitations of the study**

The short duration of mitosis provides a technical challenge to conclusively demonstrate whether some of our findings, such as the phosphorylation of RIPK3 by PLK1, occur precisely in the G2 phase or continue in mitosis. Additionally, while we back most of our findings in MEFs, L929 cells are used in a few experiments. L929 cells are unique in their necroptotic response and the demonstration of these findings warrants further investigation in other cell lines. Lastly, we use staurosporine to show that increased G2/M apoptosis is not a general tendency of RIPK3-independent apoptosis which shares common executioner caspases such as caspase 3. Staurosporine suffers from the drawback that it causes intrinsic apoptosis. While a trigger of extrinsic apoptosis such as cycloheximide + TNF $\alpha$  has been used in past in some studies, in our own

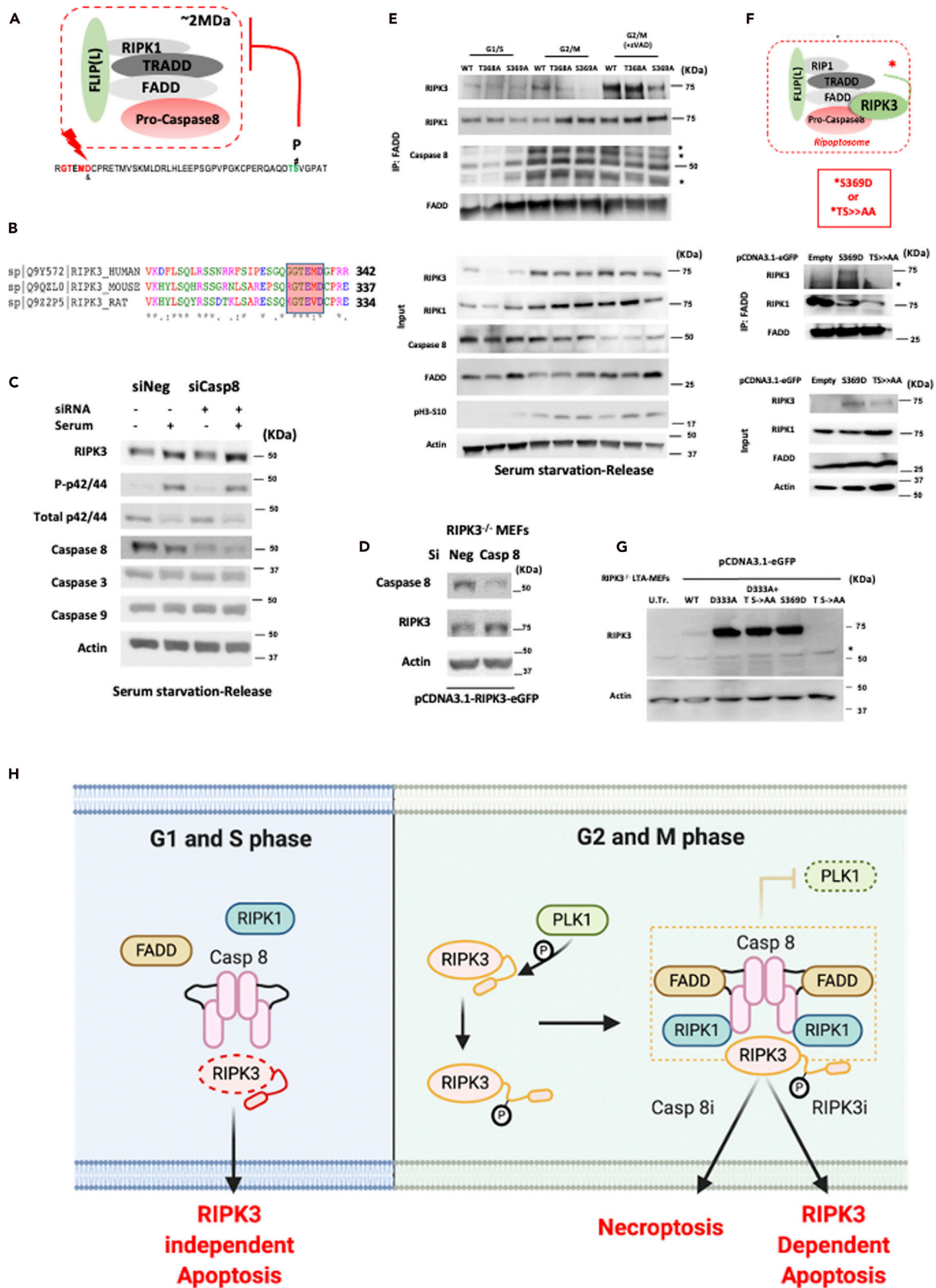


**Figure 6. S369 phosphorylation prevents ripoptosome-mediated cleavage of RIPK3**

(A) Schematic representation of the interaction of ripoptosome with RIPK3. PLK1 consensus site on RIPK3 (green) and caspase cleavage consensus site (red), as well as key residues D333 (&) and S369 (#) are marked.  
 (B) ClustalW analysis was performed on human, mouse and rat RIPK3, and the region indicating the conserved caspase 8 cleavage site is presented.  
 (C) L929 cells were transfected with siRNA against non-specific target (siNeg) or caspase 8 (siCasp8) in serum free media for 36h. Serum was added to indicated samples 10h before harvest. Samples were harvested and analyzed by western blotting.  
 (D) RIPK3-eGFP expressing *Ripk3*<sup>-/-</sup> MEFs were transfected with siRNA against non-specific target (siNeg) or caspase 8 (siCasp8). Cell-lysates were prepared 36h post-transfection and analyzed by western blotting.  
 (E) *Ripk3*<sup>-/-</sup> LTA-MEFs expressing RIPK3-eGFP with the indicated substitutions are serum starved and released for 10h. Indicated samples are treated with 20μM zVAD upon release. Immunoprecipitation with FADD is performed followed by western blotting for indicated proteins in the IP and input fractions.  
 (F) Schematic outline depicting RIPK3 mutants. *Ripk3*<sup>-/-</sup> MEFs were transfected with pCDNA3.1-eGFP, S369D or T368A S369A (TS >> AA). IP was performed using antibody against FADD and western blotting was performed for indicated proteins on IP and input fractions.  
 (G) *Ripk3*<sup>-/-</sup> LTA-MEFs were transiently transfected with the indicated constructs or left un-transfected (U.Tr.). 36h post-transfection, cells were harvested for western blotting with the indicated antibodies.  
 (H) Model summarizing the kinetics of RIPK3 in the cell cycle. Cells in the G1 and S phases express basal amounts of RIPK3 and therefore are comparatively less prone to necroptosis and RIPK3-dependent apoptosis. As cells enter the cell cycle and advance toward G2 and later M phases, PLK1 phosphorylates RIPK3 at S369. This phosphorylation enables RIPK3 to be incorporated inside the ripoptosome, which is naturally assembled during mitosis. Depending on the stimulus (inhibition of RIPK3 kinase activity, or caspase 8 ablation), RIPK3 can trigger apoptosis and necroptosis upon release from ripoptosome. PLK1 is degraded by the ripoptosome as demonstrated by Liccardi et al. \*non-specific bands

experiments, cycloheximide interferes with non-apoptotic processes in the cell including abrogation of RIPK3 synthesis itself, rendering the analysis of apoptosis technically challenging.

**Resource availability**

*Lead contact*

Further information and requests for resources and reagents should be directed to and will be fulfilled by the lead contact, Bo Liu ([liub@surgery.wisc.edu](mailto:liub@surgery.wisc.edu)).

*Materials availability*

All unique/stable reagents generated in this study are available from the lead contact with a completed Materials Transfer Agreement.

*Data and code availability*

The study did not generate any new data sets.

**METHODS**

All methods can be found in the accompanying [Transparent methods supplemental file](#).

**SUPPLEMENTAL INFORMATION**

Supplemental information can be found online at <https://doi.org/10.1016/j.isci.2021.102320>.

**ACKNOWLEDGMENTS**

The authors would like to acknowledge Dr. Satish Sekhar for assistance in vector constructions and critical discussions. The authors also acknowledge Nihal Voruganti and Dr. Sahil Chaudhary for technical assistance and Dr. Sarah Franco for critical reading of the manuscript. We acknowledge the help of Dr. Grzegorz Sabat at proteomics-mass spectrometry facility at the UW-Biotech center. Graphical abstract created with BioRender.com. This study was supported by the National Institutes of Health R01HL088447 (BL) and R01HL122562 (BL), and American Heart Association 17PRE33670082 (KG). The funders had no role in study design, data collection and analysis, decision to publish, or preparation of the manuscript.

**AUTHOR CONTRIBUTIONS**

K.G. and B.L. designed the study. K.G. performed research and generated new reagents. K.G. and B.L. analyzed the data and wrote the manuscript.

**DECLARATION OF INTERESTS**

The authors declare no conflict of interest.

Received: June 30, 2020  
Revised: September 23, 2020  
Accepted: March 15, 2021  
Published: April 23, 2021

## REFERENCES

- Allan, L.A., and Clarke, P.R. (2007). Phosphorylation of caspase-9 by CDK1/cyclin B1 protects mitotic cells against apoptosis. *Mol. Cell* 26, 301–310.
- Altieri, D.C. (2003). Survivin, versatile modulation of cell division and apoptosis in cancer. *Oncogene* 22, 8581–8589.
- Badie, C., Itzhaki, J.E., Sullivan, M.J., Carpenter, A.J., and Porter, A.C. (2000). Repression of CDK1 and other genes with CDE and CHR promoter elements during DNA damage-induced G(2)/M arrest in human cells. *Mol. Cell. Biol.* 20, 2358–2366.
- Cai, Z., Jitkaew, S., Zhao, J., Chiang, H.C., Choksi, S., Liu, J., Ward, Y., Wu, L.G., and Liu, Z.G. (2014). Plasma membrane translocation of trimerized MLKL protein is required for TNF-induced necroptosis. *Nat. Cell Biol.* 16, 55–65.
- Castedo, M., Perfettini, J.L., Roumier, T., Andreau, K., Medema, R., and Kroemer, G. (2004). Cell death by mitotic catastrophe: a molecular definition. *Oncogene* 23, 2825–2837.
- Chen, W., Wu, J., Li, L., Zhang, Z., Ren, J., Liang, Y., Chen, F., Yang, C., Zhou, Z., Su, S.S., et al. (2015). Ppm1b negatively regulates necroptosis through dephosphorylating Rip3. *Nat. Cell Biol.* 17, 434–444.
- Chen, W., Zhou, Z., Li, L., Zhong, C.Q., Zheng, X., Wu, X., Zhang, Y., Ma, H., Huang, D., Li, W., et al. (2013). Diverse sequence determinants control human and mouse receptor interacting protein 3 (RIP3) and mixed lineage kinase domain-like (MLKL) interaction in necroptotic signaling. *J. Biol. Chem.* 288, 16247–16261.
- Choi, S.W., Park, H.H., Kim, S., Chung, J.M., Noh, H.J., Kim, S.K., Song, H.K., Lee, C.W., Morgan, M.J., Kang, H.C., et al. (2018). PELI1 selectively targets kinase-active RIP3 for ubiquitylation-dependent proteasomal degradation. *Mol. Cell* 70, 920–935 e7.
- Degterev, A., Hitomi, J., Germscheid, M., Ch'en, I.L., Korkina, O., Teng, X., Abbott, D., Cuny, G.D., Yuan, C., Wagner, G., et al. (2008). Identification of RIP1 kinase as a specific cellular target of necrostatins. *Nat. Chem. Biol.* 4, 313–321.
- Degterev, A., Huang, Z., Boyce, M., Li, Y., Jagtap, P., Mizushima, N., Cuny, G.D., Mitchison, T.J., Moskowitz, M.A., and Yuan, J. (2005). Chemical inhibitor of nonapoptotic cell death with therapeutic potential for ischemic brain injury. *Nat. Chem. Biol.* 1, 112–119.
- Dondelinger, Y., Aguilera, M.A., Goossens, V., Dubuisson, C., Grootjans, S., Dejardin, E., Vandebaele, P., and Bertrand, M.J. (2013). RIPK3 contributes to TNFR1-mediated RIPK1 kinase-dependent apoptosis in conditions of cIAP1/2 depletion or TAK1 kinase inhibition. *Cell Death Differ.* 20, 1381–1392.
- Eckerdt, F., and Strebhardt, K. (2006). Polo-like kinase 1: target and regulator of anaphase-promoting complex/cyclosome-dependent proteolysis. *Cancer Res.* 66, 6895–6898.
- Feng, S., Yang, Y., Mei, Y., Ma, L., Zhu, D.E., Hoti, N., Castanares, M., and Wu, M. (2007). Cleavage of RIP3 inactivates its caspase-independent apoptosis pathway by removal of kinase domain. *Cell Signal.* 19, 2056–2067.
- Feoktistova, M., Geserick, P., Kellert, B., Dimitrova, D.P., Langlais, C., Hupe, M., Cain, K., Macfarlane, M., Hacker, G., and Leverkus, M. (2011). cIAPs block Ripoptosome formation, a RIP1/caspase-8 containing intracellular cell death complex differentially regulated by cFLIP isoforms. *Mol. Cell* 43, 449–463.
- Frank, T., Tuppi, M., Hugle, M., Dotsch, V., Van Wijk, S.J.L., and Fulda, S. (2019). Cell cycle arrest in mitosis promotes interferon-induced necroptosis. *Cell Death Differ.* 26, 2046–2060.
- Liccardi, G., Ramos Garcia, L., Tenev, T., Annibaldi, A., Legrand, A.J., Robertson, D., Feltham, R., Anderton, H., Darding, M., Peltzer, N., et al. (2019). RIPK1 and caspase-8 ensure chromosome stability independently of their role in cell death and inflammation. *Mol. Cell* 73, 413–428 e7.
- Lin, J., Li, H., Yang, M., Ren, J., Huang, Z., Han, F., Huang, J., Ma, J., Zhang, D., Zhang, Z., et al. (2013). A role of RIP3-mediated macrophage necrosis in atherosclerosis development. *Cell Rep.* 3, 200–210.
- Lindon, C., and Pines, J. (2004). Ordered proteolysis in anaphase inactivates Plk1 to contribute to proper mitotic exit in human cells. *J. Cell Biol.* 164, 233–241.
- Luedde, M., Lutz, M., Carter, N., Sosna, J., Jacoby, C., Vucur, M., Gautheron, J., Roderburg, C., Borg, N., Reisinger, F., et al. (2014). RIP3, a kinase promoting necroptotic cell death, mediates adverse remodeling after myocardial infarction. *Cardiovasc. Res.* 103, 206–216.
- Mandal, P., Berger, S.B., Pillay, S., Moriwaki, K., Huang, C., Guo, H., Lich, J.D., Finger, J., Kasparcova, V., Votta, B., et al. (2014). RIP3 induces apoptosis independent of proinflammatory kinase activity. *Mol. Cell* 56, 481–495.
- Matthess, Y., Raab, M., Knecht, R., Becker, S., and Strebhardt, K. (2014). Sequential Cdk1 and Plk1 phosphorylation of caspase-8 triggers apoptotic cell death during mitosis. *Mol. Oncol.* 8, 596–608.
- McQuade, T., Cho, Y., and Chan, F.K. (2013). Positive and negative phosphorylation regulates RIP1- and RIP3-induced programmed necrosis. *Biochem. J.* 456, 409–415.
- Meng, L., Jin, W., Wang, Y., Huang, H., Li, J., and Zhang, C. (2016). RIP3-dependent necrosis induced inflammation exacerbates atherosclerosis. *Biochem. Biophys. Res. Commun.* 473, 497–502.
- Micheau, O., and Tschopp, J. (2003). Induction of TNF receptor I-mediated apoptosis via two sequential signaling complexes. *Cell* 114, 181–190.
- Muller, G.A., Stangner, K., Schmitt, T., Wintsche, A., and Engeland, K. (2017). Timing of transcription during the cell cycle: protein complexes binding to E2F, E2F/CLE, CDE/CHR, or CHR promoter elements define early and late cell cycle gene expression. *Oncotarget* 8, 97736–97748.
- Newton, K., Dugger, D.L., Wickliffe, K.E., Kapoor, N., De Almagro, M.C., Vucic, D., Komuves, L., Ferrando, R.E., French, D.M., Webster, J., et al. (2014). Activity of protein kinase RIPK3 determines whether cells die by necroptosis or apoptosis. *Science* 343, 1357–1360.
- Oberst, A., Dillon, C.P., Weinlich, R., McCormick, L.L., Fitzgerald, P., Pop, C., Hakem, R., Salvesen, G.S., and Green, D.R. (2011). Catalytic activity of the caspase-8-FLIP(L) complex inhibits RIPK3-dependent necrosis. *Nature* 471, 363–367.
- Pucci, B., Kasten, M., and Giordano, A. (2000). Cell cycle and apoptosis. *Neoplasia* 2, 291–299.
- Roychowdhury, S., McMullen, M.R., Pisano, S.G., Liu, X., and Nagy, L.E. (2013). Absence of receptor interacting protein kinase 3 prevents ethanol-induced liver injury. *Hepatology* 57, 1773–1783.
- Shin, S., Sung, B.J., Cho, Y.S., Kim, H.J., Ha, N.C., Hwang, J.I., Chung, C.W., Jung, Y.K., and Oh, B.H. (2001). An anti-apoptotic protein human survivin is a direct inhibitor of caspase-3 and -7. *Biochemistry* 40, 1117–1123.
- Su, L., Quade, B., Wang, H., Sun, L., Wang, X., and Rizo, J. (2014). A plug release mechanism for membrane permeation by MLKL. *Structure* 22, 1489–1500.
- Sun, L., Wang, H., Wang, Z., He, S., Chen, S., Liao, D., Wang, L., Yan, J., Liu, W., Lei, X., et al. (2012). Mixed lineage kinase domain-like protein mediates necrosis signaling downstream of RIP3 kinase. *Cell* 148, 213–227.
- Tenev, T., Bianchi, K., Darding, M., Broemer, M., Langlais, C., Wallberg, F., Zachariou, A., Lopez, J., Macfarlane, M., Cain, K., et al. (2011). The Ripoptosome, a signaling platform that assembles in response to genotoxic stress and loss of IAPs. *Mol. Cell* 43, 432–448.
- van de Weerd, B.C., Van Vugt, M.A., Lindon, C., Kaur, J.J., Rozendaal, M.J., Klompaker, R., Wolthuis, R.M., and Medema, R.H. (2005).

Uncoupling anaphase-promoting complex/cyclosome activity from spindle assembly checkpoint control by deregulating polo-like kinase 1. *Mol. Cell Biol.* 25, 2031–2044.

Vitner, E.B., Salomon, R., Farfel-Becker, T., Meshcheriakova, A., Ali, M., Klein, A.D., Platt, F.M., Cox, T.M., and Futerman, A.H. (2014). RIPK3 as a potential therapeutic target for Gaucher's disease. *Nat. Med.* 20, 204–208.

Wang, H., Sun, L., Su, L., Rizo, J., Liu, L., Wang, L.F., Wang, F.S., and Wang, X. (2014). Mixed lineage kinase domain-like protein MLKL causes necrotic membrane disruption upon phosphorylation by RIP3. *Mol. Cell* 54, 133–146.

Wang, Q., Liu, Z., Ren, J., Morgan, S., Assa, C., and Liu, B. (2015). Receptor-interacting protein kinase 3 contributes to abdominal aortic aneurysms via smooth muscle cell

necrosis and inflammation. *Circ. Res.* 116, 600–611.

Wang, Q., Zhou, T., Liu, Z., Ren, J., Phan, N., Gupta, K., Stewart, D.M., Morgan, S., Assa, C., Kent, K.C., et al. (2017). Inhibition of receptor-interacting protein kinase 1 with Necrostatin-1s ameliorates disease progression in elastase-induced mouse abdominal aortic aneurysm model. *Sci. Rep.* 7, 42159.

iScience, Volume 24

## **Supplemental information**

**PLK1-mediated S369 phosphorylation  
of RIPK3 during G2 and M phases enables  
its ripoptosome incorporation and activity**

**Kartik Gupta and Bo Liu**

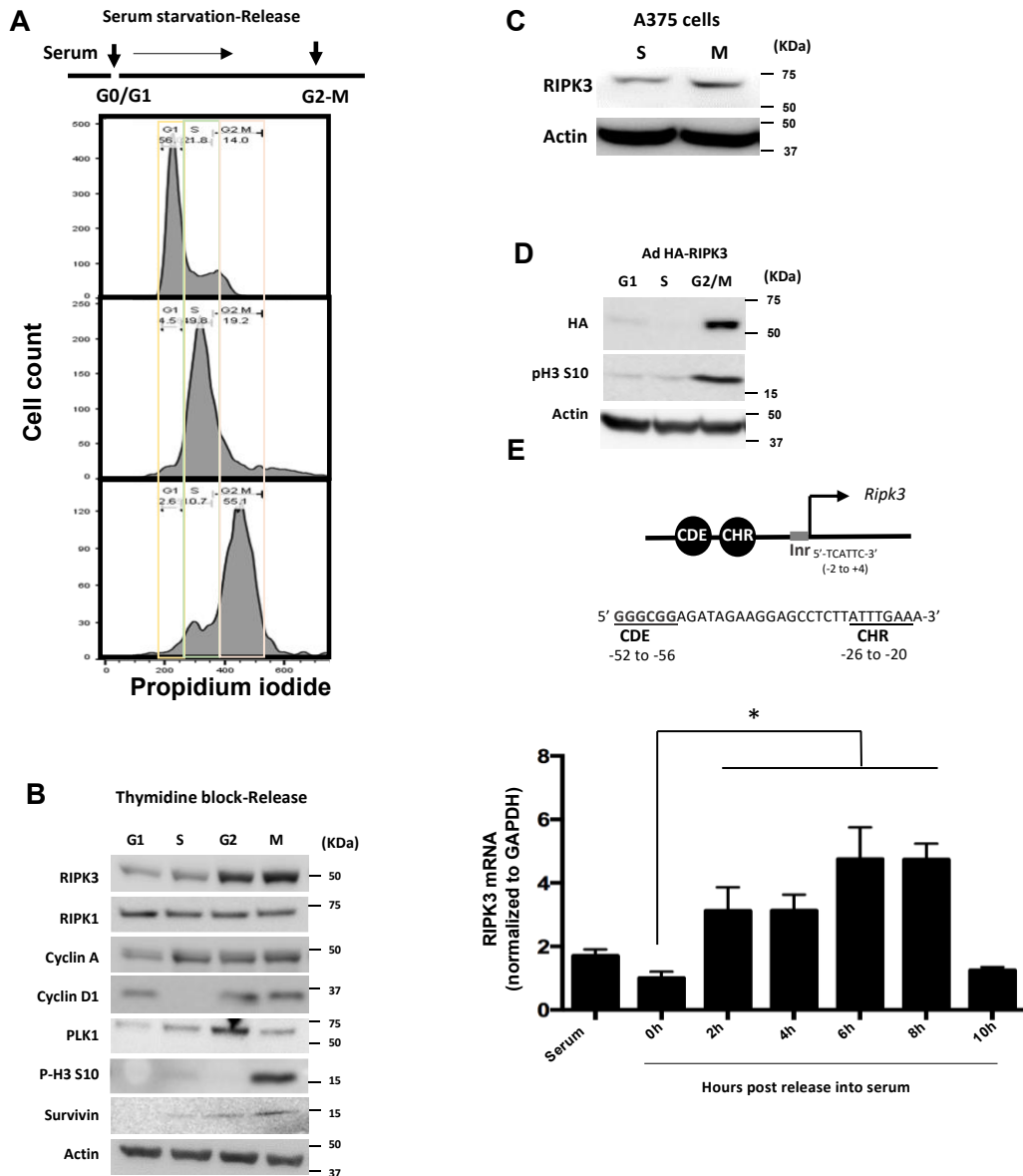


**Figure S1: RIPK3 is a component of the ripoptosome during G2/M phases, Related to Figure 1.** A) (up) scheme of serum-starvation- release. (low) L929 cells were serum-starved for 36h or released for 5h or 10h, fixed in ethanol and stained with PI. Cell-cycle was analyzed by flow-cytometry. B) L929 cells were synchronized to the G1, S, G2 and M phases by double thymidine block and release-method. Lysates were prepared from cells harvested in each phase and analyzed by western blotting. C) Human A375 cells were synchronized using double-thymidine block-release and relative RIPK3 levels were assayed for using western blotting. D)

L929 cells were arrested by addition of thymidine and simultaneously infected with adenoviruses encoding HA-RIPK3 (M.O.I of 1000) for 24h. Cells were left arrested (G1-phase) or released from thymidine for 3h (S-phase) or 8h (G2/M-phase) after which the cells were lysed and RIPK3 levels were analyzed using western blotting. E) Schematic representation of putative cis-promoter elements in the proximal *Ripk3* promoter, showing the cell cycle-dependent element (CDE) and the cell cycle genes homology region (CHR) as well as the initiator (Inr) element. (Below) L929 cells were serum starved for 36h and indicated samples were released by the addition of 10% (v/v) serum. Samples were harvested at various time-points after release and *Ripk3* mRNA was analyzed using RT-qPCR. *Ripk3* mRNA was normalized to GAPDH and fold change is relative to 0h starved cells. \* $p < 0.05$ ; using one-way ANOVA.

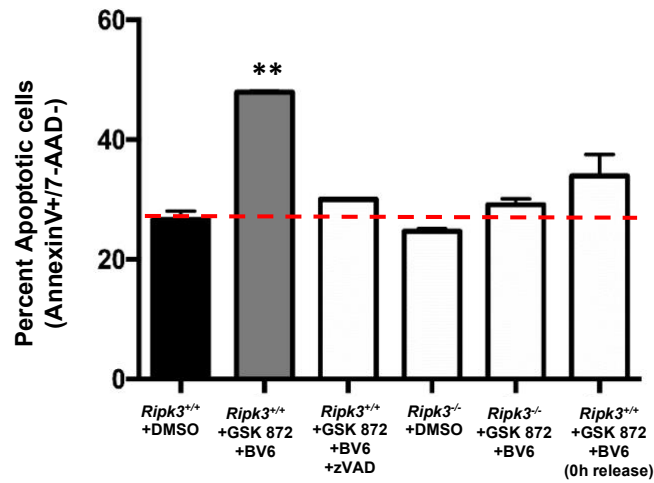
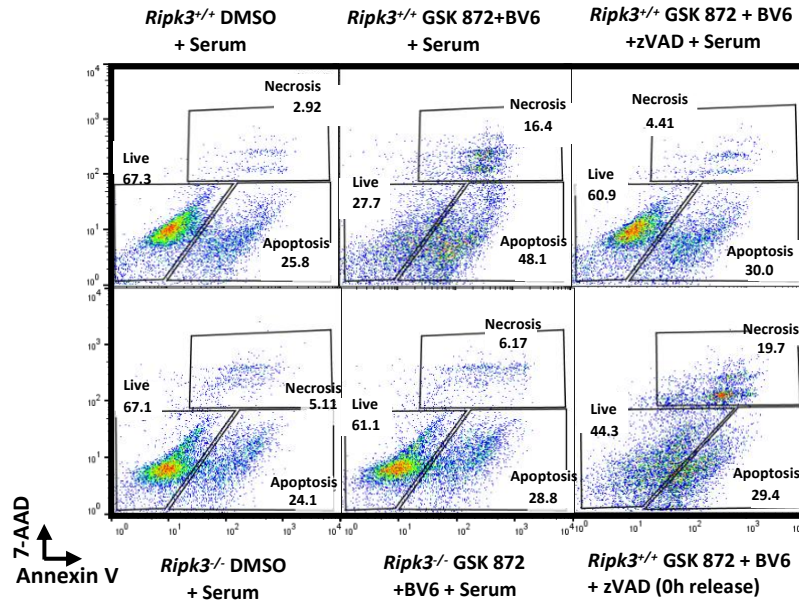


**Figure S2: G2/M phases are associated with increased RIPK3-mediated apoptosis, Related to Figure 2.** *Ripk3*<sup>+/+</sup> or *Ripk3*<sup>-/-</sup> MEFs were synchronized by serum starvation and released for 16h by the addition of 10% serum. 3h before harvesting cells, 10  $\mu$ M GSK'872 was added along with 20  $\mu$ M zVAD and 10  $\mu$ M BV6 where indicated. Cell death was evaluated by flow cytometry. Bar graph shows percent apoptosis (Annexin V+/ 7-AAD-) and necrosis (Annexin V+/ 7-AAD+).

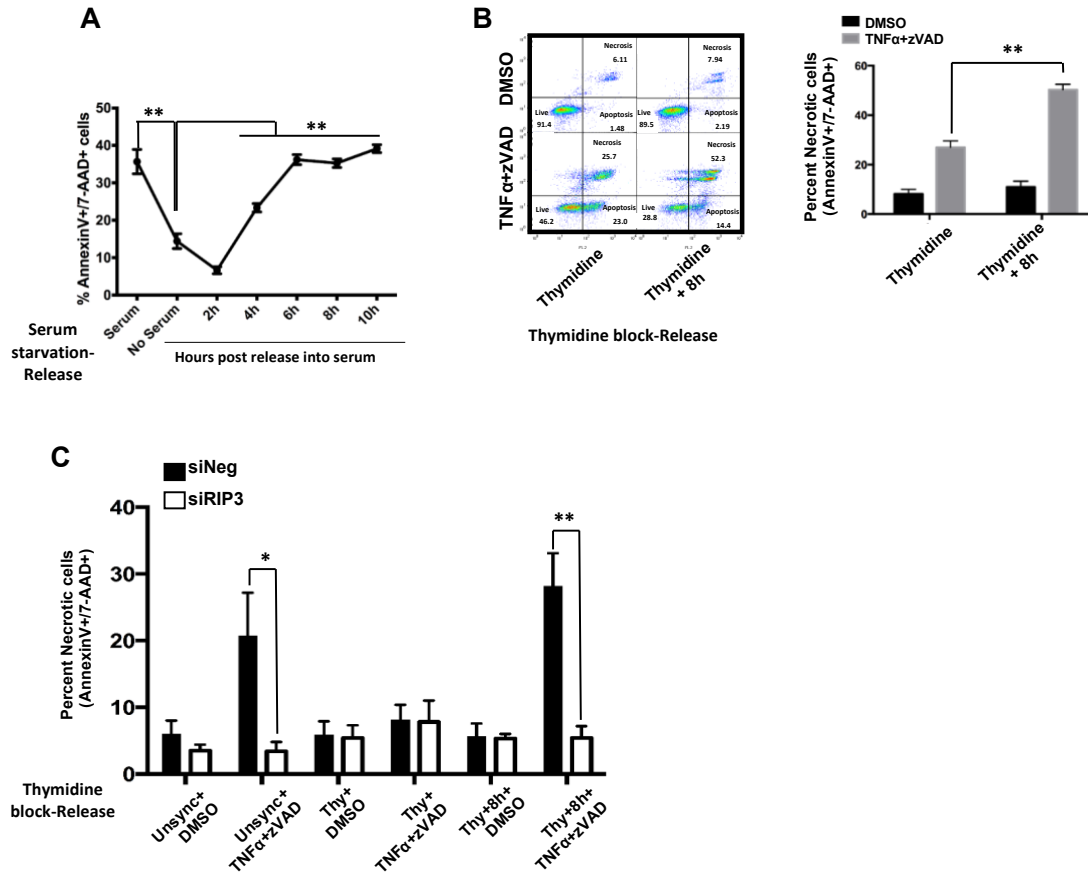


**Figure S3: RIPK3 is restrained inside the ripoptosome but retains its pro-necrotic kinase activity, Related to Figure 3.** A) Following serum-starvation and release-based synchronization, L929 cells were released for indicated time points. 2h prior to harvest, cells were treated with 10 ng/mL TNF $\alpha$  +20  $\mu$ M zVAD. Necroptosis was measured using flow cytometry. Statistical comparisons are shown relative to no serum cells. B) Double thymidine block and release method was utilized to synchronize L929 cells. At the end of the second thymidine block, cells were left in thymidine (thymidine) or released by adding fresh media for 8h (thymidine + 8h). Cell death was evaluated by flow cytometry after treatment with DMSO or 10 ng/mL TNF $\alpha$  +20  $\mu$ M zVAD for 2h. Bar graph shows percent necrotic cells. C) Cells were treated with non-targetting control (siNeg) or siRNA targeting RIPK3 (siRIPK3). Following double-thymidine block and release as in (B), cells were treated for 2h with DMSO or 10 ng/mL TNF $\alpha$  + 20  $\mu$ M zVAD and necrosis was measured using flow cytometry. \* $p$ <0.05; \*\* $p$ <0.01 using one-way (A) or two-way ANOVA.

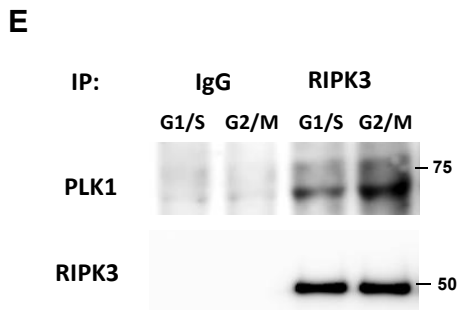
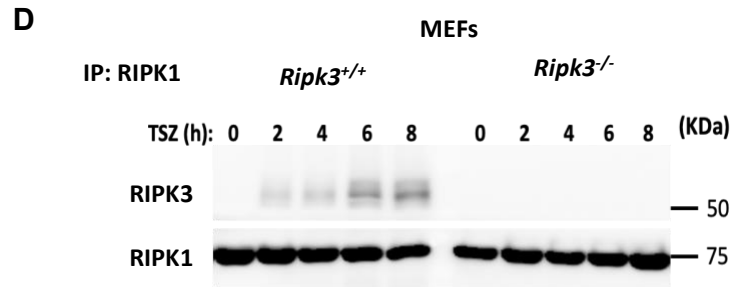
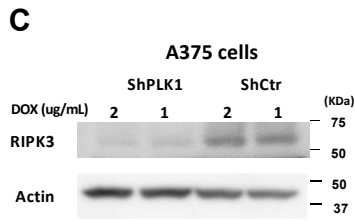
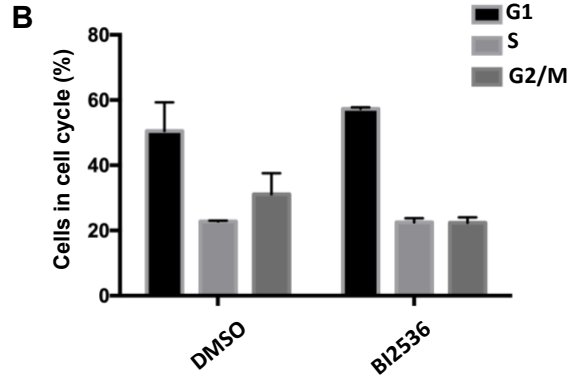
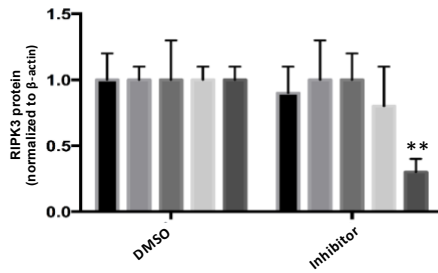
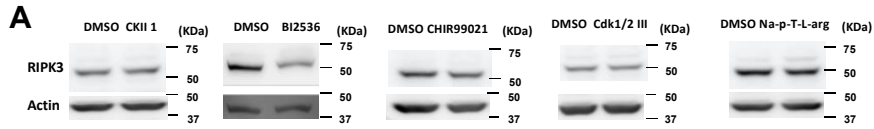


**Figure S4: PLK1 activity is essential for RIPK3 stability, Related to Figure 4.** A) L929 cells were treated with the indicated inhibitors or DMSO for 36h. RIPK3 levels were analyzed by western blotting. Bar graph shows RIPK3 protein levels normalized to beta actin and fold change is relative to DMSO treated groups. B) PI staining and flow cytometry based analysis was performed on cells treated with DMSO or BI2536 as in (A) and result from cell cycle analysis is presented. C) A375 cells stably expressing a dox-inducible PLK1 construct or non-targeting construct (ShCtr) were treated with 1 or 2 ug/mL doxycycline for 36h and RIPK3 levels were measured by western blotting. D) RIPK1 was immunoprecipitated from RIPK3<sup>+/+</sup> and RIPK3<sup>-/-</sup> cells and western blotting is performed. E) Immunoprecipitation using isotype control (IgG) or RIPK3 was performed. Indicated factors were probed using western blotting. Absence of PLK1 in IgG led us to conclude the specific nature of this interaction. All data shown are mean  $\pm$  SD of three independent experiments. \*\*p<0.01 using one-way ANOVA.

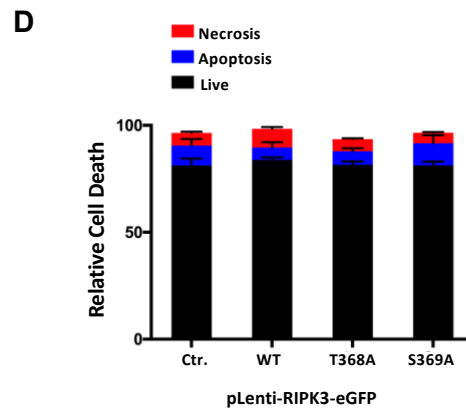
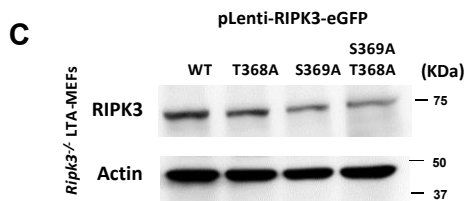
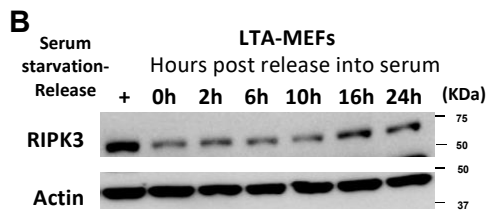
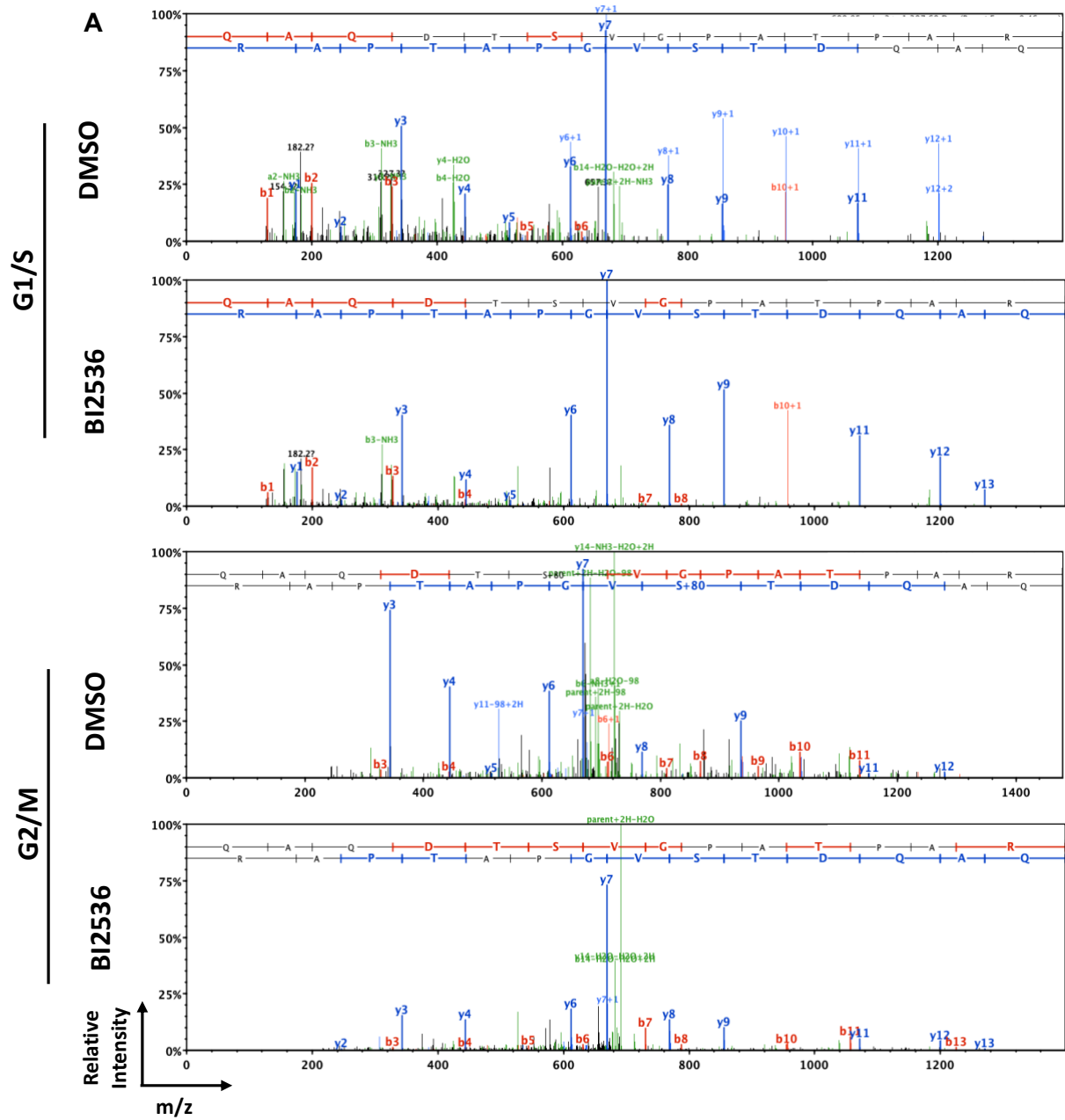


**Figure S5: PLK1 associates with and phosphorylates RIPK3 at S369, Related to Figure 5.**

A) Cells were synchronized by double-thymidine block and treated with DMSO or BI2536. IP was performed using RIPK3 antibody and analyzed by mass-spectrometry. The intensity is plotted against m/z for the tryptic digest in RIPK3 (R)QAQDTSVGPATPAR(T), highlighting a subset of fragments y8/y9. The y8/y9 fragments demonstrate the increased m/z in DMSO that is absent from BI2536 treated samples and G1/S phase samples. B) MEFs were serum starved for 48h and released from serum starvation by addition of FBS to a final concentration of 10%. Cells were harvested at indicated time points post release into serum and analyzed by western blotting with indicated antibodies. Experiments were repeated at least three times. C) *Ripk3*<sup>-/-</sup> LTA-MEFs were infected with lentiviruses encoding RIPK3-GFP (WT) or the indicated amino acid substitutions. Cells were selected in puromycin and were analyzed for RIPK3 expression in an asynchronous population. D) *Ripk3*<sup>-/-</sup> LTA-MEFs were infected with lentiviruses encoding empty (Ctr.), RIPK3-GFP (WT) or the indicated amino acid substitutions and analyzed for cell death using Annexin V-PE and 7-AAD based flow cytometry. No significant differences are observed among samples.

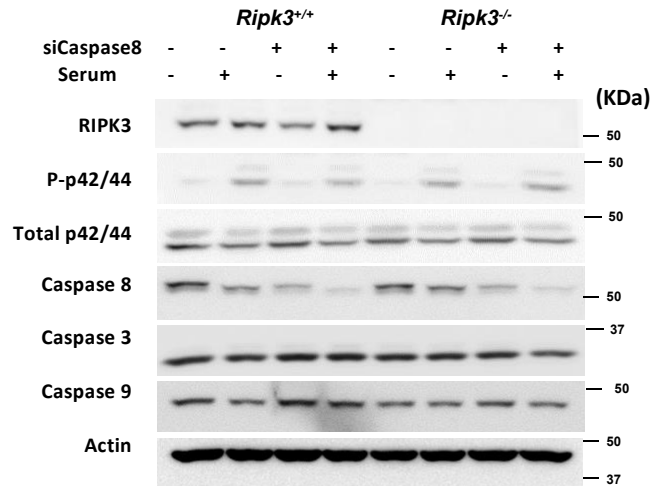


**Figure S6: S369 phosphorylation limits caspase-mediated degradation of RIPK3, Related to Figure 6.** Serum free media was added to MEF cells and were simultaneously transfected with the indicated siRNAs. 36h after serum withdrawal, indicated cells were released by the addition of 10% FBS (v/v) for 16h (MEFs). Samples were prepared for western blotting and indicated antibodies are used.

Putative Kinase/ Enzyme	Inhibitor used	Organism	Position	Sequence
<b>GSK3β</b>	CHIR99021	Mouse	308-315	HYLSQHRS
		Rat	305-312	HYLSQYRS
		Human	303-310	HYLSQLRS
<b>CDK</b>	CDK1/2 inhibitor III	Mouse	371-377	GPATPAK
		Rat	396-401	RGTTPR
		Human	415-422	GTPSPGPR
<b>CK2</b>	CKII inhibitor I	Mouse	318-324	RNLSARE
		Rat	315-321	TKLSARE
		Human	313-319	RRFSIPE
<b>D-box (APC/C)</b>	Na-p-tosyl-L-arg	Mouse	243-251	SRPPLTELP
		Rat	240-248	RRPPLTELP
		Human	238-246	NRPSLAELP
<b>PLK1</b>	BI2536	Mouse	366-372	QDTSVGP
		Rat	366-372	KEASFGH
		Human	399-405	PETSTFR

**Table 1: Eukaryotic linear motif analysis demonstrating predicted kinases/ post translational modifiers for RIPK3, Related to Figure 4.**

## Transparent Methods

### Cell culture and synchronization

L929 cells were cultured in DMEM medium (4.5 g/L glucose) under 10% FBS (unless stated otherwise) and 1% penicillin-streptomycin in a humidified chamber at 37°C under 5% CO<sub>2</sub>. For synchronization studies, cells were seeded at 40% confluence and after attachment to the culture plate, 2.5 mM of thymidine (Sigma Aldrich, St. Louis, MO) was added for 16h from 250 mM stock prepared in sterile water. Cells were washed 2X with DPBS and fresh medium was added. For nocodazole block, 100 ng/mL nocodazole was added 3 hours after release; for double-thymidine block, 2.5 mM thymidine was added for an additional 16 hours then the cells were either harvested in G1/S or released for harvest in G2 and M phases of the cell cycle. Mouse embryonic fibroblasts were isolated from E12.5 mice (*Ripk3<sup>+/+</sup>* and *Ripk3<sup>-/-</sup>*) and cultured on T175 flasks under conditions described above in addition to supplementation with L-glutamine. MEF cells were immortalized by infecting with lentiviruses encoding SV40 large T antigen (LTA-MEFs; lentiviruses encoding LTA are a kind gift from Siddhant Jain, University of Wisconsin- Madison). A375 cells were a kind gift from Dr. Nihal Ahmad (University of Wisconsin- Madison). Reagents used include TNF $\alpha$  (R&D Systems Minneapolis, MN), Z-VAD-FMK (Bachem, Torrance, CA), hoechst (Thermo Fisher Scientific, MA), propidium iodide, cycloheximide, thymidine, nocodazole, CDK1/2 inhibitor III, N $\alpha$ -p-Tosyl-L-arginine methyl ester hydrochloride, CKII inhibitor I, CHIR99021, GSK'843 (Aobious, Gloucester, MA), GSK'872 (BioVision, Milpitas, CA). Smac mimetic BV6 (Apexbio, Boston, MA). The siRNAs were prepared in OptiMEM (Thermo Fisher Scientific, MA) and Lipofectamine RNAiMax (Thermo Fisher Scientific, MA) reagent and were used as per manufacturer's instructions. The siRNA used include RIPK3, PLK1 and AllStars negative (Qiagen, Valencia, CA).

### **Flow-cytometry for cell death analysis**

Cell death was measured by using an Annexin V-PE and 7-AAD staining Kit (BD Biosciences, San Jose, CA). Cultures were rinsed with PBS and incubated with 0.25% trypsin at 37°C for 2 min. The detached cells (from culture medium, PBS wash, and trypsin treatment) were collected by centrifugation (2000 rpm, 5 min). Cell pellets were further washed twice with PBS and resuspended in 1 mL 1X binding buffer from the Annexin V-PE/7-AAD staining Kit. 5 uL of PE Annexin-V and 5uL of 7-AAD were added to the cells and incubated at room temperature for 15 min. After incubation, 400 uL binding buffer was added to each sample. Cells were analyzed using a Becton Dickinson Biosciences FACS Calibur (BD Biosciences, San Jose, CA). The population is represented as percent of Annexin V-PE<sup>+</sup> and 7-AAD<sup>+</sup> cells (Annexin V<sup>+</sup>/7-AAD<sup>+</sup>).

### **Western blotting**

Cells were lysed in RIPA buffer (Sigma-Aldrich, St. Louis, MO) containing 1X protease and phosphatase inhibitors (Halt Cocktail, Thermo Scientific, Rockford, IL). After BCA-based protein quantification, equal amounts of protein extract were loaded and separated by SDS-PAGE and then transferred to polyvinylidene fluoride (PVDF) membranes. The membranes were blocked for 45 min at room temperature with 5% skim milk in TBS plus 0.1% Tween 20, and then incubated with primary antibodies overnight at 4°C, followed by HRP-labeled secondary antibodies. Labeled proteins were visualized with an enhanced chemiluminescence system (PerkinElmer-cetus, Boston, MA) and ImageQuant LAS 4000 Mini (GE Healthcare Bio-Sciences, P.O. Pittsburgh, PA). For quantification, densities of bands were determined by ImageJ (National Institute of Health, Bethesda, MD). The antibodies used are anti-RIPK3 (ProSci, Poway, CA), anti-RIPK1 (BD Biosciences, San Jose, CA), anti-RIPK3 (human), anti-P-p42/44, anti-caspase 8, anti-caspase 3, anti-p-Histone 3 Serine 10, anti-cyclin D1 (all from Cell Signaling Technologies, Danvers, MA), anti-PLK1 (Santa Cruz Biotechnology, CA for confocal microscopy; Upstate, MA for proximity ligation assay and western blotting). anti-FADD, anti-Survivin (Santa Cruz Biotechnology), anti-

beta actin (Sigma, St. Louis, MO). Anti- cyclin A (Abcam, Cambridge, MA). Horseradish Peroxidase (HRP)-conjugated Antibodies were purchased from Bio-Rad (Hercules, CA). All primary antibodies were used at 1:1000 dilution and secondary antibodies at 1:10,000 dilution.

### **RNA Isolation and Quantitative Real-Time PCR (RT-qPCR)**

Total RNA was extracted from cultured cells using Trizol reagent (Life Technologies, Carlsbad, CA) according to manufacturer's instructions. 2 µg total RNA was used for the first-strand cDNA synthesis (Applied Biosystems, Carlsbad, CA). RT-qPCR was carried out using the 7500 Fast Real-Time PCR System (Applied Biosystems, Carlsbad, CA). Each cDNA template was amplified in triplicate using SYBR Green PCR Master Mix (Applied Biosystems, Carlsbad, CA) with gene specific primers. QuantiTect Primers purchased from Qiagen (Valencia, CA) were used for amplification of cDNA. The relative mRNA levels were calculated using the  $2^{-\Delta\Delta CT}$  method. GAPDH was used as an endogenous control.

### **Kinase Assay**

The kinase assay was set in a reaction volume of 6µL. For each reaction, 25 ng of recombinant mouse PLK1 (stock 350 ng/µL, Sinobiological Cat# 50624-M07B) was incubated with 100 ng of full length mouse recombinant RIPK3 (stock 800 ng/µL, Cat # LS-G23474) in Kinase Buffer I (Signal Chem Cat # K23-09) containing a working concentration of 5 mM MOPS (pH7.2), 2.5 mM β-glycerol phosphate, 5 mM MgCl<sub>2</sub>, 1 mM EGTA, 0.4 mM EDTA and 0.25 mM DTT (Signal Chem). Kinase reaction was made to proceed by the addition of 50 µM ultrapure ATP (250 µM stock, Promega). As a control, PLK1 inhibitor BI2536 was added at a final concentration of 30 nM to the indicated lane. The reaction was allowed to proceed for 1h at 30°C. The reaction was stopped by the addition of 5X loading dye consisting of SDS and 12.5% β-ME followed by boiling at 95°C for 10 min. The lysates were run on a denaturing gel (TGX Stain Free gel, BioRad, Hercules, CA) and total protein was assayed for by placing the gel on a UV transilluminator as

per the manufacturer's instructions. After transfer onto PVDF membrane and blocking in 5% milk + TBST, the membrane was assayed for total P-Serine (SCBT Cat# sc81514).

### **Co-immunoprecipitation assay**

Co-immunoprecipitation was performed for endogenous (L929) protein or exogenously expressed constructs in 293T cells. After indicated treatment, cells were lysed in Pierce IP-lysis buffer (Thermo Fisher Scientific, MA) supplemented by protease phosphatase inhibitors and quantified using BCA method of protein quantification as described above. 2.5-5 µg antibody per reaction was used to perform Co-IP and 1-2 mg total protein was used per IP sample. Protein A or G magnetic Sure Beads (Biorad, Hercules, CA) were used as per manufacturer's instructions. Incubations were performed for 30 min between beads+ antibody and 4h between lysate+ antibody on beads at room temperature as per the manufacturer's suggested protocol. The IP fraction was eluted in Laemmli buffer (950 ul + 50 uL β-ME) and proteins were separated on polyacrylamide gel followed by transfer onto PVDF membrane, blocking and primary antibody incubation overnight (see western blotting). The following day, the membranes were processed as described above except CleanBlot secondary antibody was used at 1:1000 dilution.

### **Confocal Microscopy and Proximity ligation assay**

An asynchronous population of L929 cells was grown on glass-slides and was fixed in 4% paraformaldehyde and washed 3X with TBST. Samples were permeabilized with 0.25% Triton X-100 and blocked in 5% BSA and 5% donkey serum for 1h at RT. Primary antibodies were added at 1:300 (RIPK3) or 1:50 (PLK1) dilution. After washing 3X with TBST, secondary antibodies were added at 1:300 dilution for 1h at RT. Samples were washed and mounted in media containing DAPI. Leica SP8 microscope was used for acquiring confocal images. Briefly, a fixed number of optical sections were acquired from different fields of cells. Images were analyzed using Coloc2 feature in ImageJ. Proximity ligation assay was used as per the manufacturer's instructions

(Sigma Aldrich, St. Louis, MO) followed by nuclear staining using DAPI. Mouse-derived anti-PLK1 and rabbit-derived RIPK3 antibodies were used for the study. Fluorescence microscopy was used to image cells and nuclear morphology based on DAPI staining was used to assign cells into the different cell cycle phases. Antibodies were used at 1:250 dilution.

### **Mass Spectrometry Analysis**

Proteins were extracted with TCA/acetone precipitation [10% TCA, 28% acetone final] then pellets re-solubilized and denatured in 7.5  $\mu$ l of 8M Urea / 50mM NH<sub>4</sub>HCO<sub>3</sub> (pH8.5) / 1mM TrisHCl for 10 minutes. Subsequently diluted to 30 $\mu$ l for reduction step with: 1.25 $\mu$ l of 25mM DTT, 2.5 $\mu$ l MeOH, 37.5 $\mu$ l 12.5mM NH<sub>4</sub>HCO<sub>3</sub> (pH8.5). Incubated at 52°C for 15 minutes, cooled on ice to room temperature then 1.5  $\mu$ l of 55mM IAA was added for alkylation and incubated in darkness at room temperature for 15 minutes. Reaction was quenched by adding 4 $\mu$ l of 25mM DTT. Subsequently 10 $\mu$ l of Trypsin:LysC solution [100ng/ $\mu$ l Trypsin:LysC mix in 25mM NH<sub>4</sub>HCO<sub>3</sub>] and 19 $\mu$ l of 25mM NH<sub>4</sub>HCO<sub>3</sub> (pH8.5) was added to 100 $\mu$ l final volume. Digestion was conducted for 2 hours at 42°C then additional 5 $\mu$ l of Trypsin:LysC solution added and digestion proceeded o/n at 37°C. Reaction was terminated by acidification with 2.5% TFA [Trifluoroacetic Acid] to 0.3% final. Mgf files were used to search against Uniprot Mus musculus amino acid sequence database with a decoy reverse entries and a list of common contaminants (43,539 mouse protein entries and 87,156 total entries) using in-house Mascot search engine 2.2.07 [Matrix Science] with variable Methionine oxidation, Serine and Threonine phosphorylation, Asparagine and Glutamine deamidation plus fixed cysteine Carbamidomethylation. Peptide mass tolerance was set at 15 ppm and fragment mass at 0.8 Da. Protein annotations, significance of identification and spectral based quantification was done with help of Scaffold software (version 4.4.1, Proteome Software Inc., Portland, OR).

### **Statistical Analysis**

Data presented are mean  $\pm$  the SD. Two-tailed Student's t-test was used when comparing two groups. One-way or two way ANOVA was used for comparison of multiple groups using GraphPad Prism. In all cases where P values for ANOVA are indicated, the global P-value is  $\leq 0.05$ .